Research Article

https://doi.org/10.1631/jzus.B2500648

Simulated microgravity suppresses oral squamous cell carcinoma growth through Piezo1-mediated regulation of calcium ion homeostasis and the autophagy pathway

Jian YUAN[1*], Yi XU[1*], Xiaocui LUO[2*], Xiaotong HE[3], Yining LI[1], Chao JIANG[4], Fan TANG[1], Shan WANG[1], Cunman HE[5], Yaohui ZHU[6], Lingkai SU[1], Hui LU[7], Shangjun ZHANG[1], Yuliu LIN[1], Keyan JI[1], Zhiyong WANG[1✉], Zuchao CAI[1✉], Qianming CHEN[1]

[1]*Stomatology Hospital, School of Stomatology, Zhejiang University School of Medicine, Zhejiang Provincial Clinical Research Center for Oral Diseases, Key Laboratory of Oral Biomedical Research of Zhejiang Province, Cancer Center of Zhejiang University, Engineering Research Center of Oral Biomaterials and Devices of Zhejiang Province, Hangzhou 310000, China*

[2]*Department of Basic Medical Sciences, School of Medicine, Tsinghua University, Beijing, China, 100084; College of Life Science, Zhejiang University, Hangzhou, Zhejiang 310058, China*

[3]*Department of Oral Maxillofacial Surgery, The First Affiliated Hospital of Zhejiang University School of Medicine, Hangzhou 310000, China*

[4]*MOE Key Laboratory of Biosystems Homeostasis & Protection, and Zhejiang Provincial Key Laboratory of Cancer Molecular Cell Biology, Life Sciences Institute, Zhejiang University, Hangzhou 310030, China*

[5]*College of Life Science, Zhejiang University, Hangzhou 310058, China*

[6]*Department of Stomatology, Yueqing Second People's Hospital, Yueqing, Wenzhou 325608, China*

[7]*Department of Orthopedics, The First Affiliated Hospital of Zhejiang University School of Medicine, Hangzhou 310000, China*

Abstract: Background: Oral squamous cell carcinoma (OSCC) is the most prevalent form of oral cancer, with metastasis significantly contributing to its poor prognosis. Emerging research indicates that microgravity may exert anti-tumor effects by inducing cell death, although the precise mechanisms remain unclear. **Methods:** The Rotary Cell Culture System (RCCS) was used to simulate microgravity, enabling observation of its effects on tumor cell proliferation and migration. Key genes and pathways influenced by simulated microgravity were identified using RNA sequencing (RNA-seq). In the tongue load-bearing tumor mouse model, we used hindlimb unloading (HU) to simulate microgravity and investigate its impact on tumor growth, and to validate the involvement of identified key genes and pathways. **Results:** Simulated microgravity induced significant morphological changes in OSCC cells, leading to the formation of multicellular spheroids and altering their biological behavior. RNA sequencing identified PIEZO1 as a key mechanosensitive gene upregulated under microgravity, along with the activation of autophagy-related pathways. In vivo experiments using a tongue load-bearing mouse model demonstrated that simulated microgravity suppressed tumor growth, which was associated with enhanced autophagy and disrupted calcium homeostasis. Piezo1 inhibition partially reversed these effects, confirming its critical role in microgravity-induced OSCC suppression. **Conclusions:** Simulated microgravity suppresses OSCC growth through Piezo1-mediated calcium dysregulation and enhanced mitophagy. Inhibition of Piezo1 reverses these effects, indicating its potential as a therapeutic target. This study highlights microgravity-based approaches as promising strategies for the treatment of OSCC.

Key words: Simulated microgravity; Mechanotransduction; Autophagy; Mitophay; Oral squamous cell carcinoma; Calcium ion homeostasis; Piezo1

✉ Zhiyong WANG, wzy0809@zju.edu.cn
Zuchao CAI, caizuchao@zju.edu.cn
* The three authors contributed equally to this work
Zhiyong WANG, https://orcid.org/0009-0004-9624-978X
Zuchao CAI, https://orcid.org/0009-0007-4500-8646

Received Oct. 16, 2025; Revision accepted Jan. 29, 2026;
Crosschecked xxx. xx, 20xx; Published online xxx. xx, 20xx

1 Introduction

Microgravity(Acres et al., 2021), experienced during parabolic flights and in orbital spacecraft and space stations, has attracted significant scientific interest since the dawn of human space exploration due to its profound effects on the human body and cellular functions.

Life on Earth has evolved under the constant influence of gravitational forces; however, the microgravity environment of space disrupts physiological processes at both the organismal and molecular levels (Lewis et al., 1998; Hughes-Fulford et al., 2015; Prasad et al., 2020b; Grimm, 2021). Studies indicate that the space environment, especially microgravity, profoundly affects cellular behavior by disrupting the balance between cellular structures and external mechanical forces, leading to molecular changes in the cytoskeleton, signal transduction, and membrane permeability(Prasad et al., 2020a). Interestingly, these cellular alterations are particularly relevant to cancer, where cells driven by genetic mutations and epigenetic changes exhibit uncontrolled growth and division(Lee and Kim, 2022). The unique conditions of microgravity may further influence these malignant cells, potentially disrupting the already fragile balance in their biological behaviors. Investigating how microgravity affects cancer cells offers a novel perspective on the complex interplay between mechanical forces and tumor progression, shedding light on potential avenues for cancer treatment.

Oral squamous cell carcinoma (OSCC) is the predominant type of head and neck cancer(Ren et al., 2020; Tan et al., 2023). The Global Cancer Observatory (GCO) project predicts an increase in OSCC incidence of around 40% by 2040, along with a rise in mortality rates (Tan, et al., 2023). Despite the existence of various therapeutic interventions for the prevention and treatment of OSCC, including chemotherapy, radiation therapy, immunotherapy, and nanomedicine, the overall 5-year survival rate for OSCC patients has remained below 50% over the past two decades (Sasahira and Kirita, 2018; Tan, et al., 2023). Therefore, the development of more effective treatment strategies is crucial for improving OSCC management and curbing malignant progression. Our prior research demonstrated that OSCC cells exhibit distinct phenotypes and growth characteristics under simulated microgravity. Based on these findings, we hypothesize that OSCC cells may possess a "gravity sensor" that converts microgravity-induced mechanical signals into biological signals, enabling mechanotransduction. Given the complexity and therapeutic challenges of OSCC, elucidating its molecular responses to external mechanical stimuli, such as microgravity, is essential for advancing treatment approaches.

Research has demonstrated that Piezo1 plays a crucial role in cellular mechanotransduction (Gudipaty et al., 2017; Nourse and Pathak, 2017). The Piezo channel family, including the Piezo1 and Piezo2 subtypes, is the first mechanosensitive cation channel identified and confirmed in mammals(Coste et al., 2010; Coste et al., 2012). Piezo1 is more broadly expressed across various human tissues, and its specific functions have been extensively elucidated over the past decade (Zong et al., 2023). Mechanical stimuli can activate Piezo1, which, when open, facilitates single-channel conductance(Lin et al., 2019). This activation mediates mechanically sensitive cation currents in diverse cell types, triggering downstream calcium signaling pathways that regulate a wide range of cellular processes(Atcha et al., 2021; Jiang et al., 2021). The mechanotransduction process mediated by Piezo1 is essential for sustaining normal cellular function. As mechanosensitive ion channels, Piezo detects changes in membrane tension. When mechanical forces act on the cell membrane, the resulting increase in membrane tension induces structural deformation of Piezo channels, thereby activating them (Xu et al., 2021). Mechanotransduction, the process by which cells sense external mechanical stimuli and convert them into biochemical signals, is a fundamental biological mechanism(Romani et al., 2021). Cellular responses to gravity represent an active form of mechanotransduction (Takahashi et al., 2021).

In this study, we demonstrate that simulated microgravity influences the biological behavior of OSCC cells and tumor regression by activating Piezo1. This activation disrupts intracellular calcium homeostasis, leading to mitochondrial calcium overload, dysfunction, and subsequent autophagy activation, providing novel insights into potential therapeutic targets for OSCC.

2 Results

2.1 Effects of SMG on the morphology and behavior of OSCC cells

To investigate the effects of simulated microgravity on OSCC cells, we conducted ground-based simulated microgravity experiments using a Rotary Cell Culture System (RCCS) bioreactor (Fig. 1a). After 48 h of cultivation under simulated microgravity (SMG), HSC-3 and HSC-4 cells in the SMG group detached from their original monolayer adhesion state. The cells adopted irregular shapes, underwent rearrangement, and reassembled into three-dimensional multicellular spheroids, exhibiting distinct three-dimensional growth characteristics (Fig. 1a).

HSC-3 cells cultured under normal gravity (NG) (Figure 1A) and horizontal rotation (HR) (Fig. 1a) exhibited typical adherent growth. Notably, when HSC-3 cells cultured under SMG were subsequently grown under normal gravity conditions (SMG-NG), those that had formed three-dimensional multicellular spheroids exhibited a re-adaptation to gravity, characterized by cell re-spreading and re-adhering to the surface (Fig. 1a; HSC-4 in Fig. S1). These findings suggest that SMG disrupts the original cell adhesion state, induces morphological changes in OSCC cells, and triggers cell deformation and reorganization, forming a novel multicellular spheroid structure.

To further assess the impact of SMG on cell viability, we conducted a CCK-8 assay to evaluate the survival rates of HSC-3 and HSC-4 cells. The results indicated a significant reduction in cell viability in the SMG group compared to the NG group at 24, 48, and 72 h ($P<0.01$, Figs. 1b and 1c). Colony formation assays further demonstrated that the SMG group exhibited a markedly reduced colony formation rate compared to the NG group ($P<0.01$, Figs. 1d and 1e), suggesting that SMG inhibits the proliferation of OSCC cells. Additionally, cell scratch experiments revealed that the migration ability of cells in the SMG group was significantly reduced compared with that in the NG group ($P<0.01$, Figs. 1f and 1g).

In summary, SMG induces morphological alterations in OSCC cells and significantly suppresses their migration and proliferation capabilities.

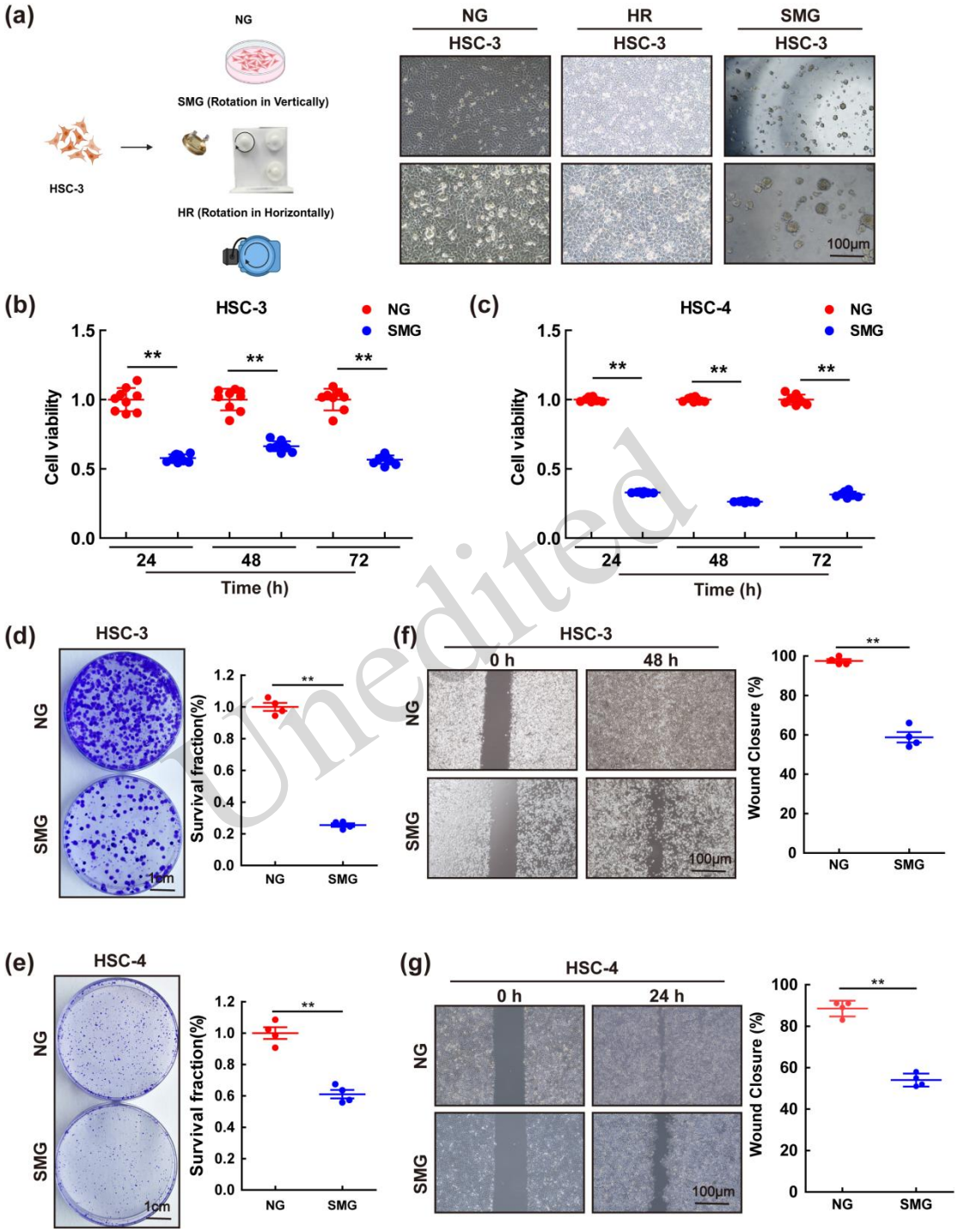

Fig. 1 Effects of simulated microgravity (SMG) on oral squamous cell carcinoma (OSCC) cell morphology and viability. (a) HSC-3 cells cultured under normal gravity (NG) conditions exhibit typical adherent growth, while cells exposed to SMG for 48 h adopt irregular shapes and reassemble into three-dimensional multicellular spheroid structures. (b, c) Cell Counting Kit-8 (CCK-8) assays show that cell viability of HSC-3 and HSC-4 cells in the SMG group was significantly reduced at 24, 48, and 72 hours compared to the NG group (n=9, *P*<0.01). (d, e) Colony formation assays indicate a marked decrease in colony formation rates under SMG conditions (n=4, *P*<0.01). (f, g) Wound healing assays demonstrate a significant reduction in the migration capability of HSC-3 and HSC-4 cells in the SMG group(n=4, *P*<0.01). Data are expressed as mean±standard deviation (SD). ns, not significant, * *P*<0.05, ** *P*<0.01.

2.2 Transcriptomic changes in OSCC under SMG: autophagy and *PIEZO1* upregulation

Next, we performed RNA sequencing (RNA-seq) on HSC-3 cells to investigate changes in gene expression under SMG conditions. Differential gene expression analysis was conducted; 2638 genes were significantly upregulated, and 2427 genes were significantly downregulated (Figs. 2a and 2b). Heatmap clustering analysis revealed significant alterations in autophagy, oxidative stress, and cytoskeletal regulation in OSCC under SMG (Fig. 2c). On the differential expression gene list, we observed a notable upregulation of mitophagy-related genes, such as ATG9A and ATG2A, as well as oxidative stress-related genes. We observed a significant upregulation of PINK1, a canonical initiator of ubiquitin-mediated mitophagy, providing further transcriptomic evidence of mitophagy activation (Fig. S2 and Table S2).

A Kyoto Encyclopedia of Genes and Genomes (KEGG) enrichment bubble plot (Fig. 2d) highlighted autophagy and mitophagy as the primary biological processes influenced by SMG in OSCC cells. A heatmap of mitophagy-associated genes revealed that the differentially expressed genes were enriched for mitophagy functions, with ATG9B as the most significant gene (Fig. 2e).

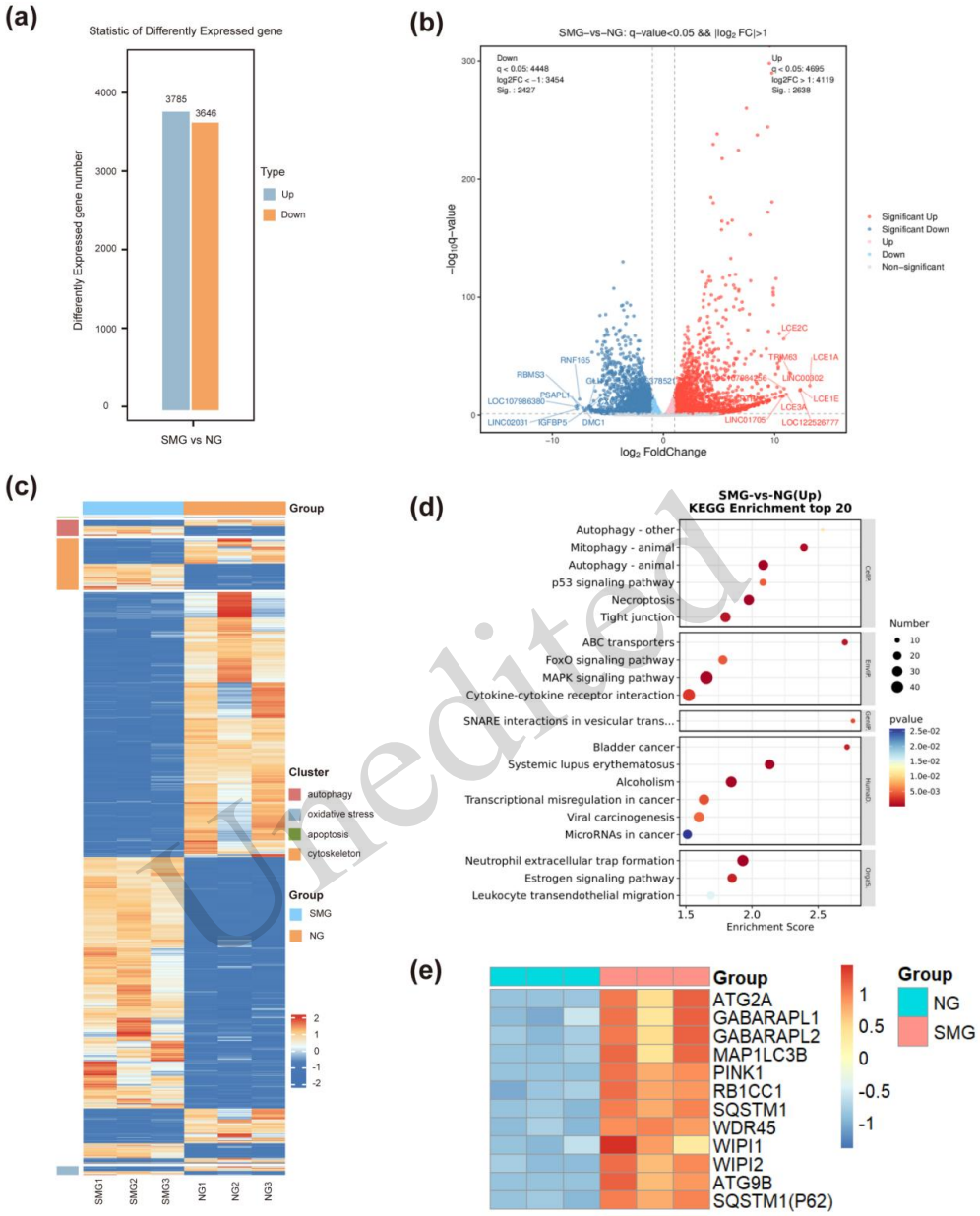

Fig. 2 RNA-seq analysis of HSC-3 cells cultured under NG and SMG conditions. (a, b) Bar and volcano plots illustrating differentially expressed genes. A total of 2638 genes were significantly upregulated, while 2427 genes were significantly downregulated. Genes with statistically significantly increased expression are highlighted in red, and those with decreased expression are shown in blue (*P*<0.05). (c) Heatmap illustrating differentially expressed genes between the NG and SMG groups, showing significant enrichment in autophagy, oxidative stress, apoptosis, and cytoskeletal regulation pathways. DESeq2-normalized counts (from three replicates per condition) were visualized using the R package heatmap. The data are column-clustered (dendrogram at the top) and row-scaled. (d) Kyoto encyclopedia of genes and genomes (KEGG) bubble plot indicating that differentially expressed genes are primarily clustered in the gene ontology (GO) terms for "Autophagy" and "Mitophagy." (e) Heatmap illustrating differentially expressed genes enriched in mitophagy function, with the most significant gene *ATG9B*. (*P*<0.001). ATG: Autophagy-Related Gene, GABARAPL1: GABA Type A Receptor Associated Protein Like 1, GABARAPL2: GABA Type A Receptor Associated Protein Like 2, MAP1LC3B: Microtubule-Associated Protein 1 Light Chain 3 Beta, PINK1: PTEN Induced Kinase 1, RB1CC1: RB1 Inducible Coiled-Coil 1, SQSTM1: Sequestosome 1, WDR45: WD Repeat Domain 45, WIPI1: WD Repeat Domain, Phosphoinositide Interacting 1, WIPI2: WD Repeat Domain, Phosphoinositide Interacting 2, ATG9B: Autophagy-Related 9B, SQSTM1(P62): Sequestosome 1 (also known as p62).

2.3 SMG-induced mitophagy in OSCC cells

A reduction in mitochondrial membrane potential (MMP) is a key indicator of mitochondrial dysfunction and is closely associated with mitophagy. Under SMG, OSCC cells exhibited decreased MMP, which in turn activated pathways promoting the selective removal of damaged mitochondria, helping to maintain cellular homeostasis. To detect changes in MMP, we used Rhodamine 123, a fluorescent probe, to measure the intensity of the fluorescence signal. Additionally, we employed CCCP, a mitochondrial uncoupler, to disrupt the electrochemical gradient across the mitochondrial membrane, further confirming the reduction in MMP.

The fluorescence intensity of HSC-3 and HSC-4 cells was analyzed using confocal fluorescence microscopy (Fig. 3a). The results revealed a significant reduction in fluorescence intensity in the SMG group compared to the NG group, resembling the effect observed in the CCCP-treated group, indicating MMP uncoupling and decreased MMP. Furthermore, cells in the SMG group exhibited abnormal nuclear morphology, including irregular size and shape, and the presence of fissures, suggesting potential nuclear damage.

Mitophagy-related protein analysis in HSC-3 cells (Fig. 3b) revealed a significant increase in the mitophagy markers ATG9B and LC3-II/LC3-I (P<0.01) and a significant decrease in P62 (P<0.01). Additionally, HSC-3 cells were infected with a dual-fluorescence autophagy lentivirus, and autophagy formation was tracked using the RFP-GFP-LC3 fusion protein under a fluorescence microscope. SMG treatment resulted in the formation of numerous autophagosomes, which were specifically localized to the mitochondria (Fig. 3c). These findings indicate that SMG induces mitophagy in OSCC cells. Analysis of differentially expressed genes (Fig. 3d) revealed a significant and robust upregulation of the mechanosensitive gene *PIEZO1* in the SMG group compared to the NG group (P<0.001). This upregulation was subsequently validated at the protein level via Western blot in subsequent in vivo experiments (see Fig. 5e and Section 2.5).

To further validate the involvement of the PINK1-PARKIN pathway, we assessed protein expression and localization. Immunofluorescence analysis revealed that SMG treatment induced significant mitochondrial recruitment of PARKIN and LC3 (Figs. S6a and S6b). Consistent with this, Western blot analysis confirmed upregulation of PINK1 and PARKIN protein levels under SMG conditions, a phenotype recapitulated by Piezo1 agonist Yoda1 (Figs. S6c and S6d).

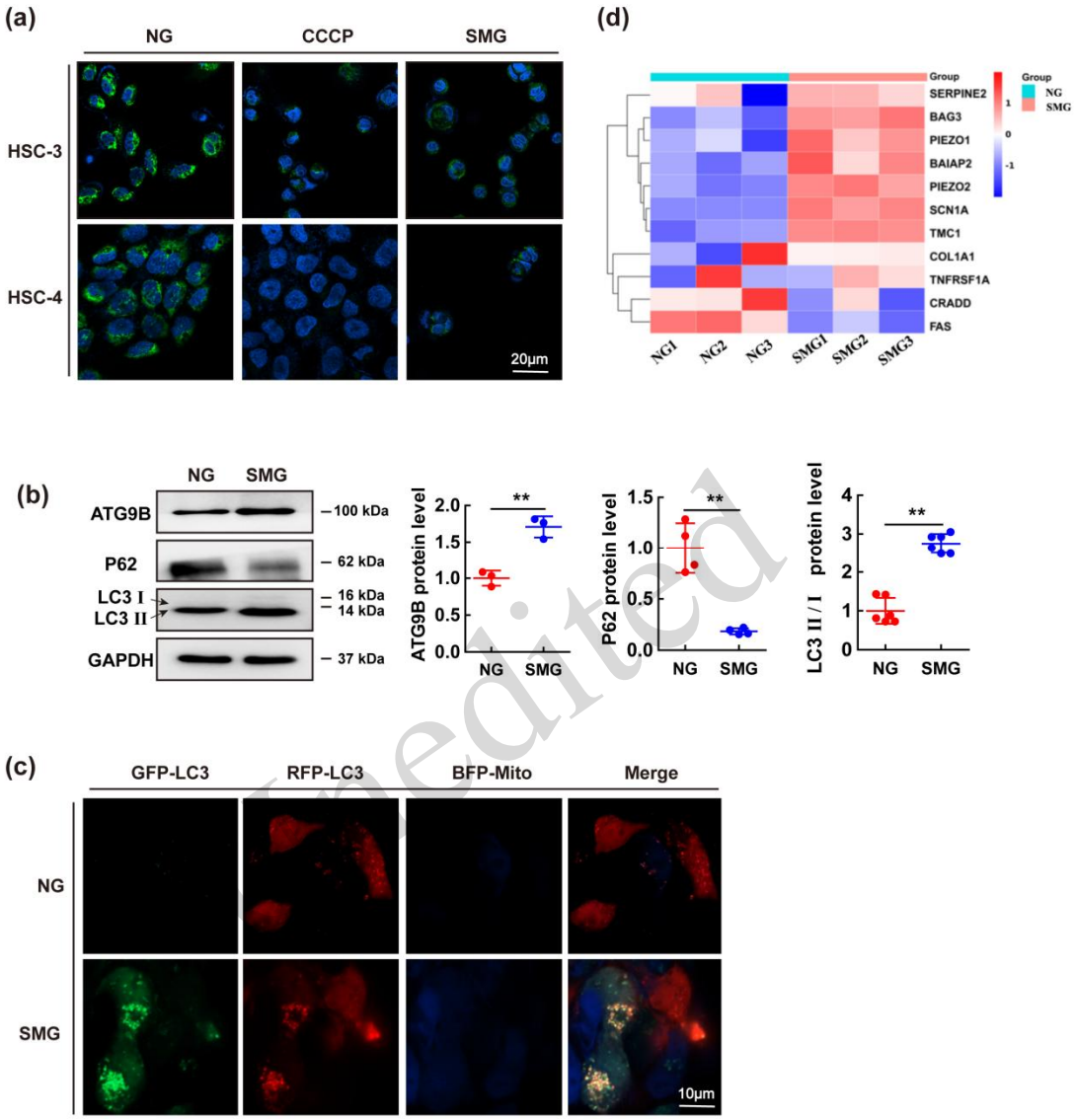

Fig. 3 SMG-induced mitophagy in OSCC cells. (a)Mitochondrial membrane potential (MMP) was assessed using Rhodamine-123 staining, with CCCP-treated cells serving as a positive control for MMP reduction. DAPI (blue) stained the nuclei, and Rhodamine-123 (green) indicated MMP. Fluorescence intensity analysis revealed a significant reduction in MMP in both OSCC cell types following SMG treatment. (b) Western blot analysis of HSC-3 cells revealed significant upregulation of mitophagy-related proteins ATG9B and LC3-II/LC3-I (P<0.01), and a marked decrease in P62 expression (P<0.01) following SMG treatment. n=4. (c) Fluorescence imaging of cells transfected with Mito (blue)-GFP-RFP-LC3 (green and red for LC3-II) via lentivirus. Following SMG stimulation, increased GFP-LC3 expression was observed, localized to the mitochondria, indicating enhanced mitophagy. (d) Heatmap illustrating key genes within the autophagy pathway, selected based on fold changes, adjusted P-values, and biological relevance. Notably, *PIEZO1* and *PIEZO2*, mechanosensitive genes associated with the cytoskeleton, were significantly upregulated in the SMG group compared with the NG group (P<0.001). Data are expressed as mean±standard deviation (SD). ns, not significant, * P<0.05, ** P<0.01. SERPINE2: Serpin Family E Member 2, BAG3: BCL2 Associated Athanogene 3, PIEZO1: Piezo Type Mechanosensitive Ion Channel Component 1, BAIAP2: BAR/IMD Domain Containing Adaptor Protein 2, PIEZO2: Piezo Type Mechanosensitive Ion Channel Component 2, SCN1A: Sodium Voltage-Gated Channel Alpha Subunit 1, TMC1: Transmembrane Channel Like 1, COL1A1: Collagen Type I Alpha 1 Chain, ATG9B: Autophagy Related 9B, P62: Sequestosome 1 (also known as SQSTM1), LC3 I: Microtubule-Associated Protein 1 Light Chain 3 Beta I, LC3 II: Microtubule-Associated Protein 1 Light Chain 3 Beta II, GAPDH: Glyceraldehyde-3-Phosphate Dehydrogenase.

2.4 Piezo1-dependent mitophagy in OSCC under SMG

Previous research has shown that SMG activates Piezo1. To further explore its effects on cellular functions, we used small interfering RNA (siRNA) to transfect HSC-3 cells and knock down Piezo1 expression, followed by assessment of its impact on cell biological behavior.

The CCK-8 assay results showed that, following SMG treatment, the survival rates of Piezo1-knockdown HSC-3 cells (siRNA-SMG) at 72 and 96 hours were significantly higher than those of the non-knockdown group (SMG) (Fig. 4a). However, similar colony formation was observed in both Piezo1-knockdown and control groups (Fig. 4b). These findings were further corroborated in HSC-4 cells (Figs. S3a and S3b). To further investigate the role of Piezo1 in cell motility, we performed wound healing assays. It was observed that the reduced migratory capacity induced by SMG was significantly restored following Piezo1 knockdown (Fig. S7b). Conversely, pharmacological activation of Piezo1 with Yoda1 was sufficient to suppress cell migration (Fig. S7c), confirming that Piezo1 acts as a negative regulator of OSCC migration under these conditions.

Mitophagy-related protein analysis in HSC-3 cells (Fig. 4c) showed that, prior to Piezo1 knockdown, SMG significantly upregulated the expression levels of mitophagy-related proteins ATG9B and LC3-II/LC3-I, while P62 expression was significantly downregulated. After Piezo1 knockdown, these changes in mitophagy-related proteins were notably attenuated, indicating the critical role of Piezo1 in SMG-induced mitophagy in OSCC cells. These findings were similarly confirmed in HSC-4 cells (Fig. S3c).

Alterations in Piezo1-mediated ion channels may affect intracellular calcium levels, such as triggering calcium influx, leading to intracellular calcium overload and further inducing mitochondria-mediated cell death (Song et al., 2022). Based on this, we hypothesize that SMG-induced mitophagy in OSCC cells may result from Piezo1-mediated calcium dysregulation. The rapid influx of calcium ions is an early indicator of mitophagy initiation. To test this hypothesis, we conducted calcium ion fluorescence assays using HSC-3 cells. This showed that, following Piezo1 knockdown, the increase in calcium ion fluorescence intensity at 30 and 60 minutes in both the SMG (siRNA-SMG) and NG (siRNA-NG) groups was significantly suppressed compared to the non-knockdown groups (NG, SMG) (Fig. 4d). This result was further validated by calcium ion fluorescence confocal imaging (Fig. S3d). Additionally, following Piezo1 activation (Yoda1), time-lapse imaging under confocal microscopy showed that mitochondrial calcium ion fluorescence intensity peaked at 180 seconds (Fig. 4e). To confirm the causal sufficiency of this pathway, cells were treated with the Piezo1 agonist Yoda1 under normal gravity. Yoda1 treatment successfully recapitulated the SMG-induced phenotype, triggering rapid calcium influx (Fig. 4e), upregulating mitophagy markers (PINK1, PARKIN, LC3-II; Fig. S6d), and suppressing cell viability and migration (Fig. S7). These gain-of-function data, combined with the loss-of-function siRNA results, solidify Piezo1 as the central mediator.

In summary, these findings suggest that under SMG, Piezo1 activation leads to calcium dysregulation in OSCC cells, resulting in mitochondrial calcium overload and subsequent mitophagy induction.

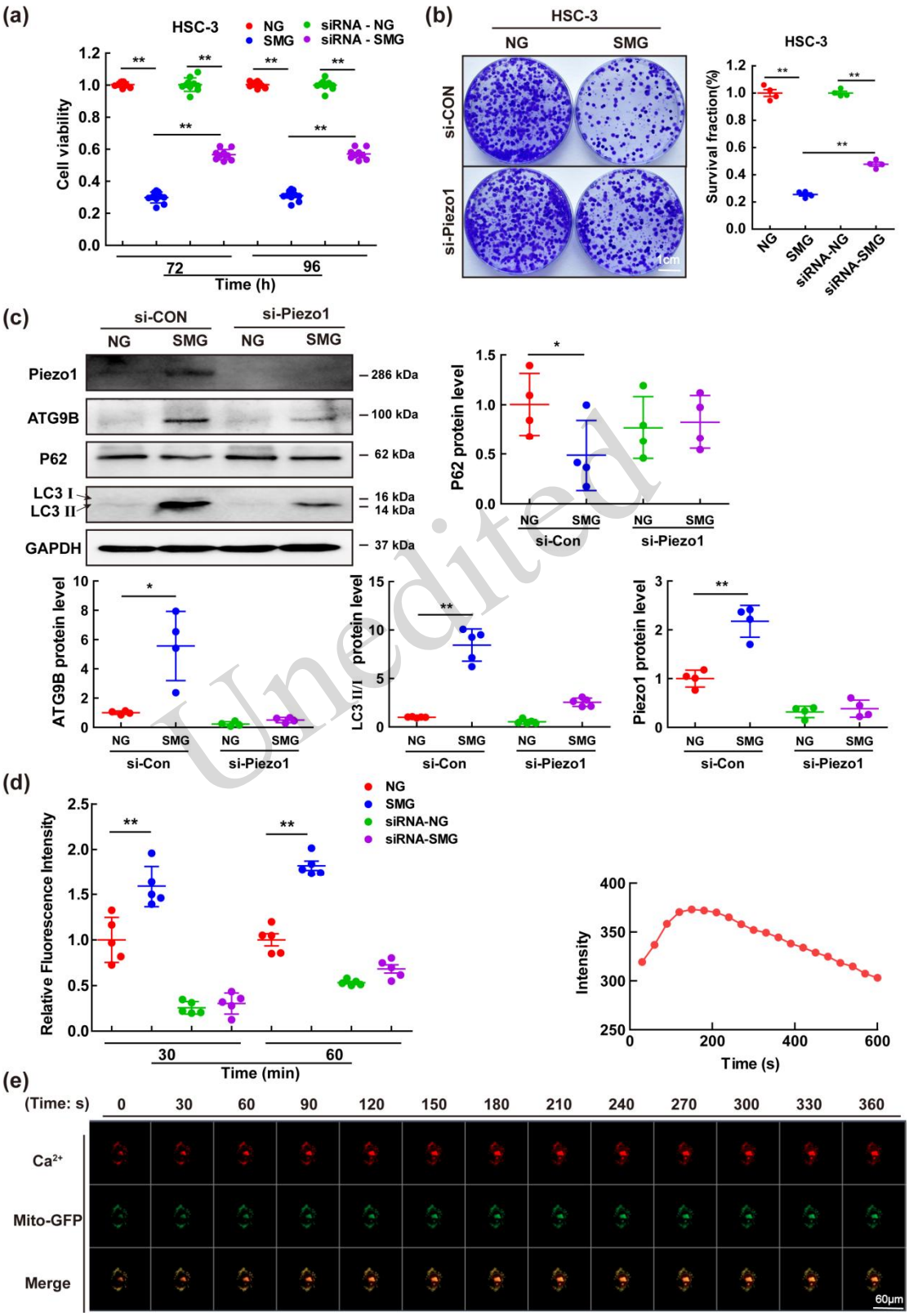

Fig. 4 SMG-induced mitophagy in OSCC cells via Piezo1 regulation (a) CCK-8 assay shows a significant reduction in cell viability under SMG conditions, which is partially restored in HSC-3 cells transfected with si-Piezo1 siRNA (n=8, *P*<0.01). (b) Colony formation assay reveals that SMG significantly decreases colony formation ability, and this reduction is

partially reversed by Piezo1 knockdown (n=4, *P*<0.01). (c) Western blot analysis of mitophagy-related proteins in HSC-3 cells. Under SMG conditions, Piezo1, ATG9B, and LC3-II/LC3-I levels are significantly upregulated, while P62 expression is reduced. Piezo1 knockdown reverses these effects (n=4, **P*<0.05, ***P*<0.01). (d) Calcium ion fluorescence assay indicates that SMG treatment markedly increases intracellular calcium levels at 30 and 60 minutes, and this effect is significantly suppressed upon Piezo1 knockdown (n=5, *P*<0.01). (e) Dynamic fluorescence imaging demonstrated a rapid rise in intracellular calcium concentration within 360 seconds after stimulation with the Piezo1 agonist Yoda1, revealing that pharmacological activation of Piezo1 with Yoda1 triggered a rapid surge in intracellular calcium, peaking at ~180 seconds. This confirmed that Piezo1 activation directly leads to calcium influx similar to that observed under SMG (the GIF images illustrating the dynamics of fluorescence intensity changes are included in the Supplementary Materials). Data are expressed as mean±standard deviation (SD). ns, not significant, * *P*<0.05, ** *P*<0.01. PIEZO1: Piezo Type Mechanosensitive Ion Channel Component 1, ATG9B: Autophagy Related 9B, P62: Sequestosome 1 (also known as SQSTM1), LC3 I: Microtubule-Associated Protein 1 Light Chain 3 Beta I, LC3 II: Microtubule-Associated Protein 1 Light Chain 3 Beta II, GAPDH: Glyceraldehyde-3-Phosphate Dehydrogenase.

2.5 SMG-induced mitophagy in OSCC tumors in vivo

We established a mouse model of OSCC by transplanting 4MOSC1 cells into the mouse tongue, and the model was successfully validated through HE staining (Figs. S4a and S4b). To simulate microgravity in tumor-bearing C57BL/6 mice, hindlimb unloading (HU) was performed using a specialized tail suspension system (Fig. 5a). The HU method is a widely recognized model for simulating microgravity, effectively mimicking the weightlessness experienced during spaceflight and its impact on various physiological systems(Globus and Morey-Holton, 2016; Grimm, 2022).

On the 10th day of simulated microgravity exposure, mice were sacrificed, and their tongues were harvested to assess tumor morphology and changes in tumor volume. The results showed a significant reduction in tumor volume in the SMG group compared with the NG group ($P<0.01$, Fig. 5b). HE staining further revealed that tumors exposed to SMG (Tumor-SMG) exhibited smaller volumes, lower tumor cell density, and reduced tumor stroma compared to tumors in the NG group (Tumor-NG) (Fig. 5c).

Furthermore, compared with the NG group, the SMG group exhibited a significant reduction in proliferating tumor cells and a marked increase in the proportion of apoptotic cells ($P<0.01$, Fig. 5d). Western blot analysis further confirmed that SMG treatment led to significant upregulation of Piezo1 expression in the SMG group ($P<0.05$), accompanied by increased levels of mitophagy-related proteins ATG9B and LC3-II/LC3-I ($P<0.01$), along with a decrease in P62 expression ($P<0.05$) (Fig. 5e). These results suggest that SMG modulates Piezo1 expression and induces mitophagy in the tumor-bearing mouse model.

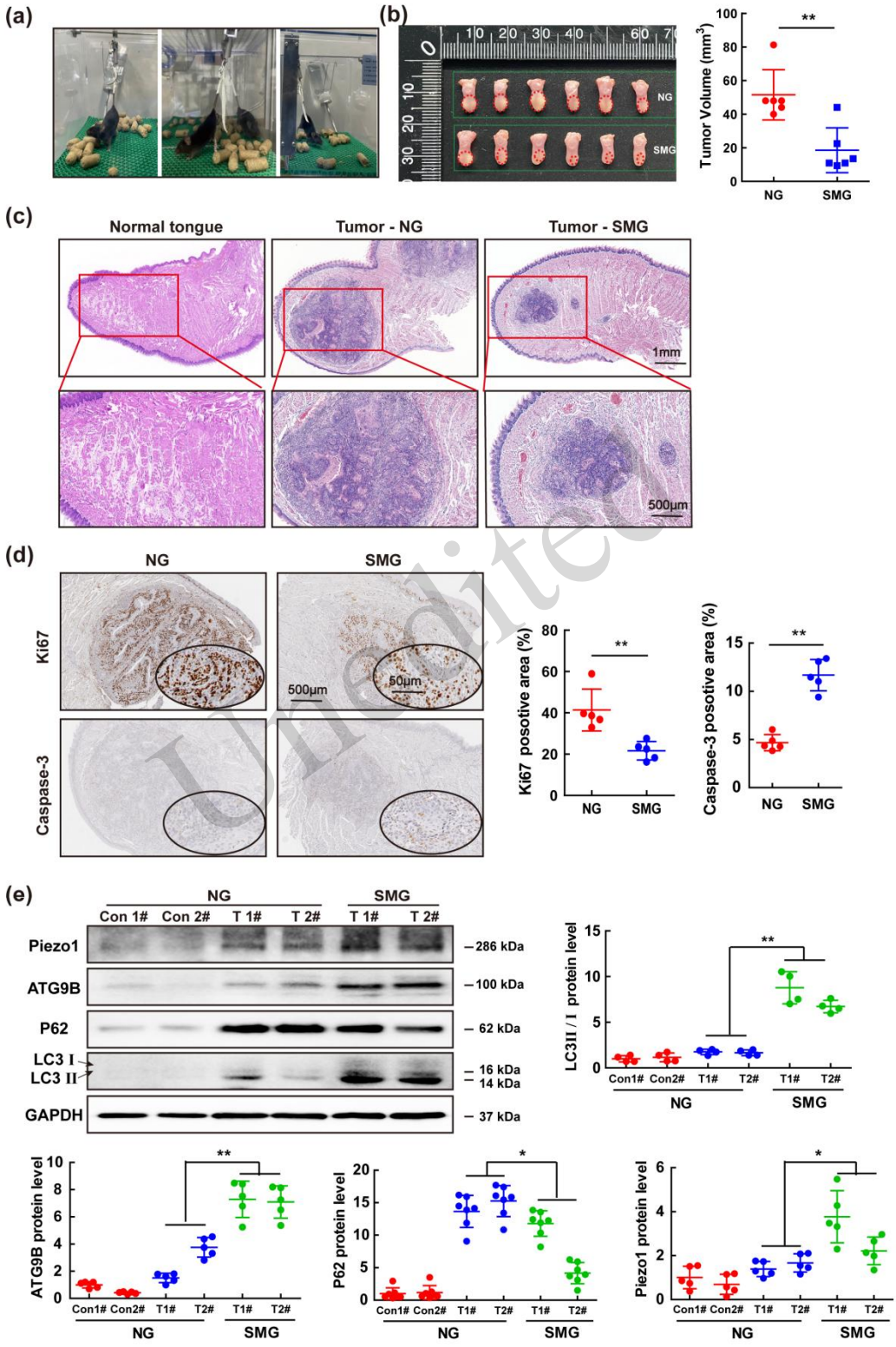

Fig. 5 SMG-induced tumor suppression and mitophagy in OSCC-bearing mice. (a) Hindlimb unloading (HU) model used to simulate microgravity in tumor-bearing mice. Tumors were induced in the tongue by cell injection, and tumor formation was validated after 7 days. Mice were then randomly assigned to NG and SMG groups, with tumor samples collected on day 10 for volume measurement. (b) Representative images of tongue tumors in the NG and SMG groups,

with tumors outlined by red dashed lines. Tumor volume was significantly smaller in the SMG group compared to the NG group (n=6, *P*<0.01). (c, d) Hematoxylin and eosin (HE) staining (c) and immunohistochemistry (IHC) (d) of tumor sections. The SMG group exhibited reduced Ki-67 expression (*P*<0.01), indicating lower proliferation, and increased Caspase-3 expression (*P*<0.01), suggesting higher apoptosis than in the NG group. n=5. (e) Western blot analysis of tumor samples revealed higher Piezo1 expression levels (n=5, *P*<0.05), P62 (n=7, *P*<0.05), ATG9B (n=5, *P*<0.01), and LC3-II/LC3-I (n=4, *P*<0.01) in the SMG group. Data are expressed as mean±standard deviation (SD). ns, not significant, * *P*<0.05, ** *P*<0.01. PIEZO1: Piezo Type Mechanosensitive Ion Channel Component 1, ATG9B: Autophagy Related 9B, P62: Sequestosome 1 (also known as SQSTM1), LC3 I: Microtubule-Associated Protein 1 Light Chain 3 Beta I, LC3 II: Microtubule-Associated Protein 1 Light Chain 3 Beta II, GAPDH: Glyceraldehyde-3-Phosphate Dehydrogenase, Ki-67: Kiel 67, Caspase-3: Cysteine-Aspartic Acid Protease 3.

2.6 Reversal of SMG effects by Piezo1 inhibition in tumor-bearing mice

Dooku1, a potent and selective antagonist of the mechanosensitive Piezo1 channel, was administered intraperitoneally at a dose of 10 mg/kg. Injections were administered to tumor-bearing mice one day before tail suspension, followed by doses on days 2, 4, 6, 8, and 10 post-suspension. Tongue tissues were harvested on day 10 (Fig. 6a).

Following Dooku1 treatment, no significant difference in tumor volume was observed between the SMG and NG control groups (ns, $P>0.05$, Fig. 6b). HE staining revealed that, after 10 days of SMG, the SMG-Dooku1 group showed no significant changes in tumor size, tumor cell density, or stromal composition compared to the NG-Dooku1 group (Fig. 6c). Likewise, assessments of cell proliferation and apoptosis revealed no significant differences between the two groups (ns, Fig. 6d). This contrasts sharply with the significant alterations seen in the absence of Dooku1 treatment ($P<0.01$, Figs. 5b-5d).

Additionally, following inhibitor administration, no significant differences in the expression levels of Piezo1, ATG9B, and P62 were observed between the SMG and NG groups ($P>0.05$). In contrast, LC3-II/LC3-I expression was significantly reduced ($P<0.01$). These results differ markedly from those observed without inhibitor treatment ($P<0.01$, Fig. 6e).

Furthermore, calcium content analysis (Fig. 6f) revealed a significant increase in calcium levels in tumor tissue in the SMG group compared with the NG group ($P<0.01$). Following treatment with Dooku1, there was no significant change in calcium ion content (ns, $P>0.05$, Fig. 6f).

In summary, inhibiting Piezo1 partially counteracted the tumor-suppressive effects of SMG in vivo.

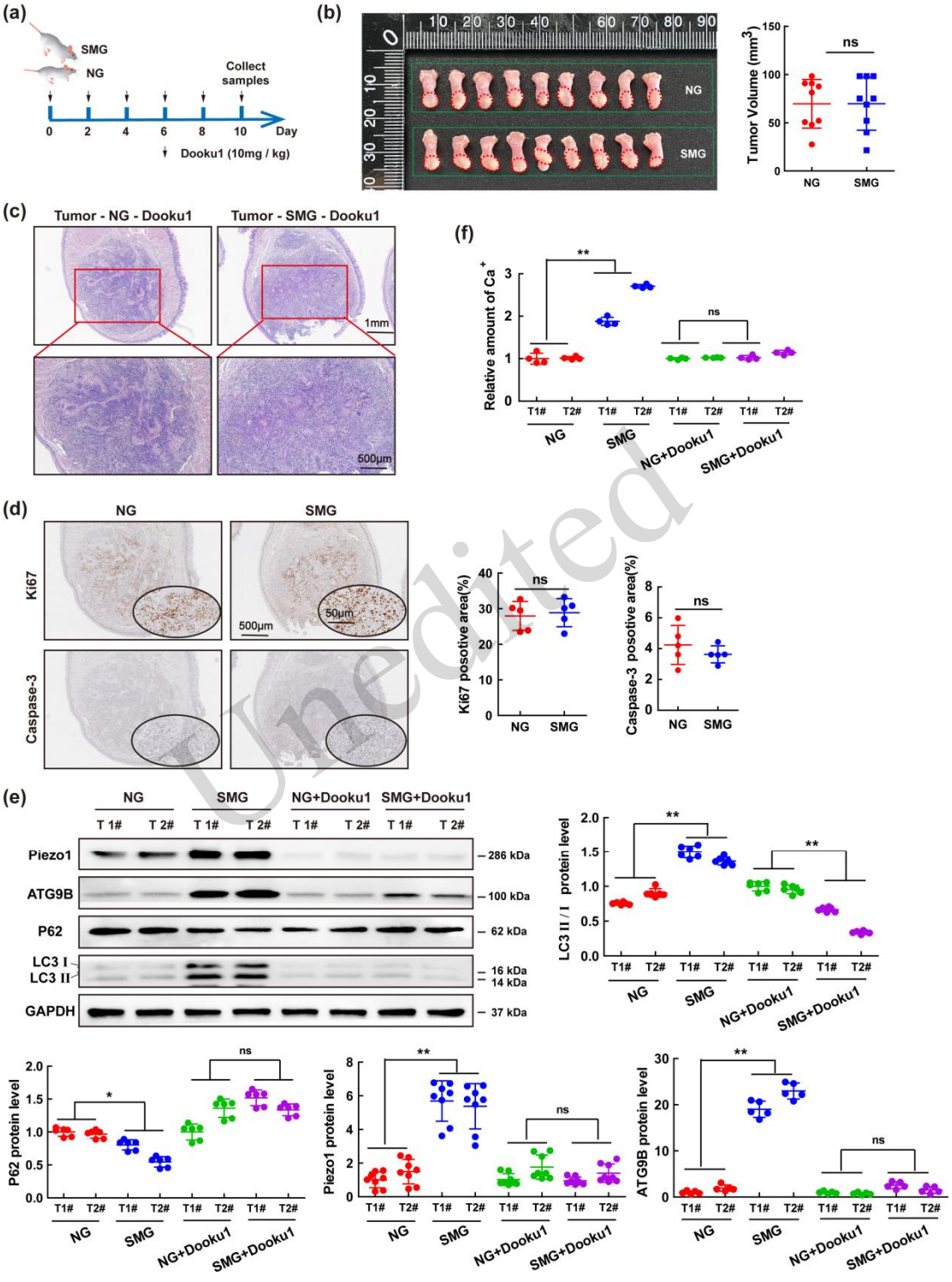

Fig. 6 Reversal of SMG-mediated tumor suppression by Piezo1 inhibitor in an OSCC mouse model. (a) Experimental timeline: Tumors were induced in the tongues of mice via cell injection. After 7 days, tumor formation was confirmed, and mice were randomly assigned to the NG and SMG groups. The HU model was used to simulate microgravity, and the Piezo1 inhibitor Dooku1 (10 mg/kg, IP) was administered on days 0, 2, 4, 6, and 8. Tumor samples were collected on day 10 to measure volume. (b) Tumor volume in the NG and SMG groups treated with Dooku1, indicated with red dashed lines.

Tumor volumes in the SMG group treated with Dooku1 were similar to those in the NG group, indicating the inhibitor's mitigating effect. n=9. (c, d) HE (c) and IHC (d) staining of tumor sections from NG and SMG groups treated with Dooku1. The IHC results showed no significant differences in Ki-67 and Caspase-3 expression between the SMG with Dooku1 and the NG groups. n=5. (e) Western blot analysis of tumor samples showed no significant differences in the expression levels of Piezo1 (n=8), ATG9B (n=5), and P62 (n=6) between the SMG and NG groups treated with Dooku1 (P>0.05). However, LC3-II/LC3-I (n=6) expression was significantly reduced (P<0.01), contrasting with the results observed without inhibitor treatment. Data are expressed as mean±standard deviation (SD). ns, not significant, * P<0.05, ** P<0.01. PIEZO1: Piezo Type Mechanosensitive Ion Channel Component 1, ATG9B: Autophagy Related 9B, P62: Sequestosome 1 (also known as SQSTM1), LC3 I: Microtubule-Associated Protein 1 Light Chain 3 Beta I, LC3 II: Microtubule-Associated Protein 1 Light Chain 3 Beta II, GAPDH: Glyceraldehyde-3-Phosphate Dehydrogenase, Ki-67: Kiel 67, Caspase-3: Cysteine-Aspartic Acid Protease 3.

3 Discussion

All life forms have evolved under the constant influence of Earth's gravity; consequently, microgravity exerts markedly different effects on cellular behavior than those experienced under the gravity conditions on Earth (Adamopoulos et al., 2021). Among these differences, the potential benefits of microgravity-induced changes in cellular behaviors for organisms remain an important area for further investigation. In this study, we demonstrated that, first, SMG alters the morphology of OSCC cells and inhibits their activity. Second, it disrupts calcium homeostasis in OSCC cells via Piezo1-mediated mechanotransduction, leading to mitochondrial calcium overload, which damages mitochondria and triggers autophagy, ultimately contributing to OSCC regression. Additionally, animal experiments further confirmed that SMG promotes OSCC regression by modulating calcium homeostasis through Piezo1-mediated pathways (Fig. 7).

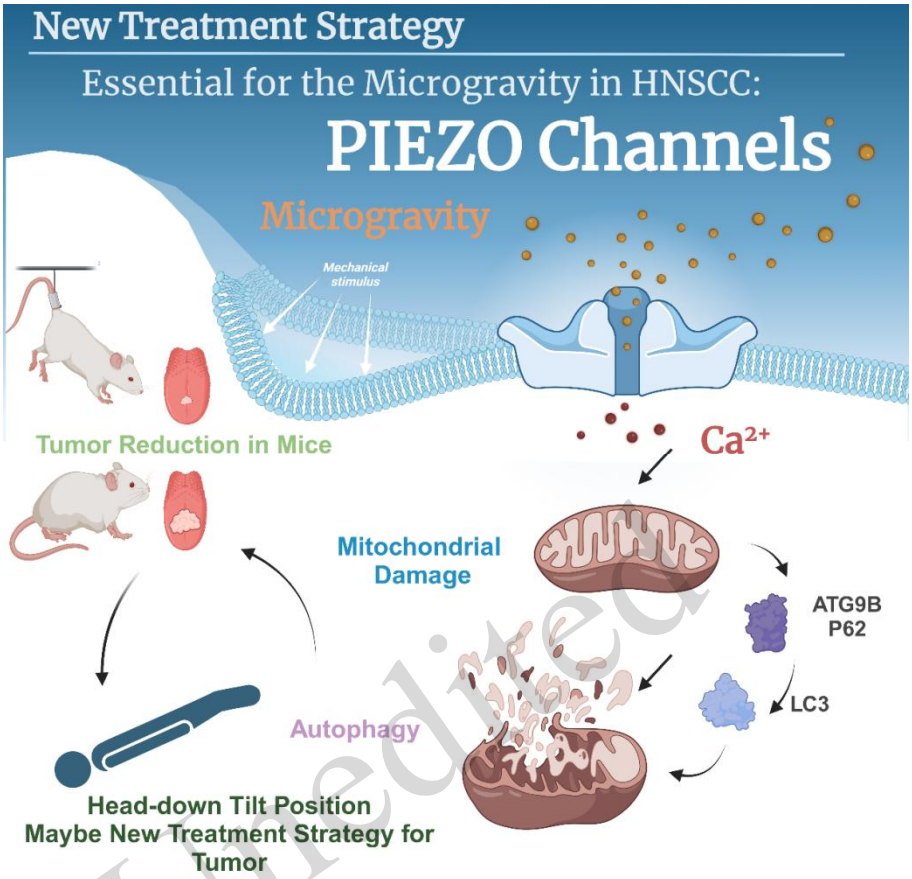

Fig. 7 Schematic diagram of the mechanism by which simulated microgravity (SMG) promotes OSCC regression. SMG acts as a mechanical stimulus to activate PIEZO1 channels, disrupting intracellular calcium homeostasis and inducing mitochondrial calcium overload. This causes mitochondrial damage, triggers autophagy (marked by LC3, ATG9B and p62), and ultimately inhibits OSCC cell activity and tumor growth. Animal experiments further validate that head-down tilt (simulated microgravity) may serve as a novel anti-tumor strategy. PIEZO1: Piezo Type Mechanosensitive Ion Channel Component 1, ATG9B: Autophagy Related 9B, P62: Sequestosome 1 (also known as SQSTM1), LC3: Microtubule-Associated Protein 1 Light Chain 3 Beta.

3.1 Piezo1 Mediates Mechanotransduction in Simulated Microgravity OSCC

A critical question remains regarding how cells convert external mechanical stimuli, such as microgravity, into intracellular biochemical signals through Piezo1-dependent mechanosensitive pathways. This study advances previous findings by elucidating a novel mechanism whereby SMG drives OSCC regression. It highlights a regulatory cascade of “mechanical force–mechanotransduction–cell fate–tumor regression” and underscores the central role of Piezo1 as a “mechanical gravity sensor”.

Piezo1 has been shown to regulate the aggressive behavior of various tumors, exhibiting either promotive or inhibitory effects depending on the cancer type and stage (Kalluri and Weinberg, 2009; Banyard and Bielenberg, 2015; Li et al., 2015; Chen et al., 2018; Suzuki et al., 2018; Friedrich et al., 2019; Han et al., 2019; Huang et al., 2019; Caulier et al., 2020; Kuntze et al., 2020; Sun et al., 2020). Our TCGA analysis (Supplementary Figure 5) revealed that Piezo1 is significantly overexpressed in tumor tissues, especially in head and neck squamous cell carcinoma (HNSCC), compared to normal tissues. Consistent with these findings, previous studies have also reported elevated Piezo1 expression in OSCC tissues and cell lines, notably in HSC-3 and HSC-4, relative to

adjacent non-cancerous tissues (Hasegawa et al., 2021). The marked overexpression of Piezo1 in OSCC, along with its increased sensitivity to microgravity-induced mechanotransduction, suggests that OSCC may respond more effectively to Piezo1-targeted therapeutic strategies than other tumors.

Microgravity significantly influences key biological behaviors of cancer cells (Kimlin et al., 2013; Vidyasekar et al., 2015; Arun et al., 2017; Deng et al., 2019; Grimm et al., 2020; Hybel et al., 2020), with substantial evidence supporting its inhibitory effects on cancer cell proliferation (Jeong et al., 2018; Bonfiglio et al., 2019; Dietz et al., 2019; Singh et al., 2021). Our study demonstrated that SMG influences OSCC progression by regulating Piezo1, suggesting that targeting Piezo1 under microgravity conditions may represent a promising therapeutic strategy.

Our study addresses this gap by investigating the effects of SMG on OSCC, proposing it as a holistic mechanobiological model. This approach offers new insights into the interplay between mechanical forces and tumor progression. Piezo1 activation by membrane deformation enables calcium influx, which regulates key tumor progression pathways, including angiogenesis, migration, and proliferation (De Stefani et al., 2012; Bootman and Bultynck, 2020; Dombroski et al., 2021). Studies show that Piezo1 activation disrupts cellular homeostasis and increases apoptosis in prostate and breast cancer cells (Hope et al., 2019; Tijore et al., 2021), suggesting it as a potential therapeutic target. In our study, SMG disrupted intracellular calcium homeostasis via Piezo1, leading to mitochondrial calcium overload and inducing mitophagy in OSCC, ultimately inhibiting tumor growth.

Amelink et al. observed significantly reduced vascular oxygenation compared with normal oral mucosa in OSCC (Amelink et al., 2008). Microgravity-induced blood redistribution may enhance oxygen levels in the maxillofacial region, potentially improving tumor oxygenation and inhibiting growth. Similarly, in the HU model, blood flow shifts towards the head, creating a hyperemic state that could alter the tumor microenvironment and synergize with SMG to affect OSCC outcomes.

In this study, it is hypothesized that microgravity-induced blood redistribution may alter the tumor microenvironment. Microvessel density (MVD) is widely recognized as a prognostic marker in cancer, with higher MVD levels often associated with poorer outcomes due to accelerated tumor growth and an increased risk of metastasis (De Palma and Hanahan, 2024) (Den Uil et al., 2019). Targeting angiogenesis has shown promise as a combination therapy strategy(Jiang and Chen, 2022), potentially reducing vascular density to limit metastatic spread(Liu et al., 2023) and reshaping the tumor microenvironment to enhance immune responses (Binnewies et al., 2018). Additionally, changes in MVD following treatment can serve as a reliable indicator of therapeutic efficacy, particularly in anti-angiogenic therapies, where reductions in MVD often reflect a favorable treatment response (Jiang, et al., 2021; Lopes-Coelho et al., 2021). In line with these concepts, we observed a reduction in MVD in OSCC, accompanied by an increase in vessel diameter. This suggests that microgravity may alter the tumor microenvironment by inhibiting angiogenesis while promoting compensatory dilation of pre-existing vessels. Although direct measurement of MVD was not the primary focus of this study, previous literature suggests that it plays a significant role in the tumor microenvironment. We propose that this vascular modulation warrants further investigation.

3.2 Advances and future directions in microgravity research for OSCC treatment

Earlier research on the effects of microgravity on biological systems focused on how gravitational changes impact physiological processes, including bone metabolism, muscle atrophy, immune function, decompression sickness, and fluid redistribution. However, the influence of microgravity on cancer remains relatively underexplored. Existing in vitro studies have demonstrated that microgravity can markedly alter tumor cell behavior, including proliferation, migration, and gene expression. Recent studies, primarily focusing on intrinsic or chemically induced signaling, have established a functional link between Piezo1 and autophagy in

other contexts; for example, Fang et al. (Fang et al., 2025), Yu et al. (Yu et al., 2025), and Hasegawa et al.(Hasegawa, et al., 2021) confirmed Piezo1's role in calcium regulation in OSCC. Current research on Piezo1 in tumors remains constrained by the absence of a comprehensive mechanobiological model. Our study advances this field by identifying 'microgravity-induced mechanical unloading' as a novel upstream stimulus. We demonstrated that SMG disrupts intracellular calcium homeostasis via Piezo1, leading to mitochondrial calcium overload and inducing mitophagy in OSCC, ultimately inhibiting tumor growth.

Looking ahead, gaining deeper insights into the molecular mechanisms modulated by microgravity could pave the way for innovative cancer therapies. In our study, the HU model in mice not only alters posture and gravity perception but also affects mechanical stress and fluid dynamics within the tumor microenvironment. These changes can reshape tumor cell morphology and function(Alvarado-Estrada et al., 2021), with postural shifts potentially leading to variations in tissue tension, thereby influencing tumor cell behavior(Massey et al., 2024). However, to fully explore whether microgravity can be harnessed for cancer treatment or prevention, further in vivo studies using microgravity models—in both animal experiments and early-phase clinical trials—are needed to establish a clearer link between rotating cell culture systems and in vivo microgravity conditions. Furthermore, the formation of multicellular spheroids observed in our SMG model suggests potential alterations in cancer cell stemness. As reviewed by Visvader and Lindeman (Visvader and Lindeman, 2012), the maintenance of cancer stemness is closely associated with therapeutic resistance and tumor metastasis.While our current RNA-seq data focused on autophagy pathways, future studies will specifically investigate stemness markers (e.g., CD44, SOX2) to determine whether microgravity-induced Piezo1 activation also regulates the cancer stem cell population.

Third, it is important to acknowledge the methodological limitations inherent in comparing 2D adherent cultures (NG) with 3D multicellular spheroids formed under simulated microgravity (SMG). As noted in recent reviews, SMG promotes the formation of scaffold-free 3D aggregates, which is a distinct phenotype of gravitational unloading [43]. However, the transition from 2D to 3D culture itself introduces variables such as altered cell–cell interactions and nutrient gradients (Breslin and O'driscoll, 2013). These structural changes may contribute to the observed omics variations independent of gravitational unloading. Future studies utilizing ground-based 3D static controls (e.g., non-adherent cultures) will be essential to further decouple the effects of dimensionality from those of microgravity.

An alternative approach to simulating microgravity in humans is the head-down tilt (HDT) bed rest model, where individuals are inclined at angles ranging from 4° to 15°, with 6° being the most commonly used in experimental settings. HDT has been employed in clinical research to study various conditions, such as acute ischemic stroke and immune responses (Ploutz-Snyder, 2016; Culliton et al., 2021), due to its effects on blood flow distribution, particularly in the head region. However, its use in cancer therapy remains limited, primarily focusing on postoperative management rather than on leveraging the therapeutic potential of HDT itself (Li et al., 2018). Exploring HDT as a non-invasive treatment strategy for head and neck tumors could represent the harnessing of gravitational principles to improve clinical outcomes.

Our study offers valuable insights into tumor progression under SMG, with findings validated using HU mouse models that closely replicate HDT conditions in humans. These results highlight Piezo1 as a promising therapeutic target. Future research will investigate the effects of true microgravity on OSCC and other head and neck tumors, and assess the potential of HDT as a treatment modality. This work aims to drive the development of innovative cancer therapies and clinical strategies that capitalize on the unique physiological responses triggered by altered gravitational conditions.

4 Conclusions

Our findings demonstrate that SMG exerts anti-tumor effects on OSCC by modulating Piezo1-mediated

calcium signaling and inducing autophagy. Piezo1 emerges as a promising target for novel therapeutic strategies that harness the unique properties of microgravity. In the future, microgravity-based approaches could pave the way for innovative cancer treatments, potentially transforming the landscape of cancer therapy and patient care. Further investigation in real microgravity environments and clinical trials will be essential for translating these insights into practical applications..

Data availability statement

The datasets generated and analyzed in the current study are available from the corresponding author upon reasonable request.

RNA-seq data files are available in GEO, accession number GSE282433.

Acknowledgement

This project has received funding from the Department of Science and Technology of Zhejiang Province (LQN25H160029, 2024ZY01032, LQ23H140003), National Natural Science Foundation of China (82301068, 82370952, 82101007), Major Project of Natural Science Foundation of Hunan Province (Open Competition, 2021JC0002), Fundamental Research Funds for the Central Universities (No.2022FZZX01-33), The Research and Development Project of Stomatology Hospital Zhejiang University School of Medicine (RD2022JCYL08, 2025DF021). This research did not receive any specific grant from funding agencies in the commercial sectors.

Author contributions

All authors have made substantial contributions to the study. Zuchao CAI and Zhiyong WANG designed the experiments and supervised the whole study. Jian YUAN, Yi XU and Xiaocui LUO performed the main research and experiments. Xiaotong HE, Yining LI, Chao JIANG, Fan TANG, Shan WANG, Cunman HE, Yaohui ZHU, Lingkai SU and Hui LU assisted with the experimental operations and sample collection. Jian YUAN and Yi XU analyzed and interpreted the experimental data. Shangjun ZHANG, Yuliu LIN and Keyan JI contributed to data curation and statistical analysis. Jian YUAN and Yi XU drafted the manuscript with the critical revision from Zuchao CAI and Zhiyong WANG . Qianming CHEN provided important academic guidance and revised the manuscript. All authors have read and approved the final version of the manuscript, have full access to all the data in the study, and take responsibility for the integrity and accuracy of the data presented.

Compliance with ethics guidelines

Jian YUAN , Yi XU, Xiaocui LUO, Xiaotong HE, Yining LI, Chao JIANG, Fan TANG, Wang SHAN, Cunman HE, Yaohui ZHU, Lingkai SU, Hui LU, Shangjun ZHANG, Yuliu LIN, Keyan JI, Zhiyong WANG, Zuchao CAI, Qianming CHEN declare that they have no conflicts of interest.

The animal experiments were performed in accordance with the protocol approved by the Animal Care and Use Committee of Zhejiang University (ETHICS CODE: ZJU20251091). All institutional and national guidelines for the care and use of laboratory animals were followed.

Declaration on the use of generative AI tools

The authors declare that no generative AI tools were used in the creation of this manuscript. All content, analysis, and writing were performed solely by the authors.

References

Acres JM, Youngapelian MJ, Nadeau J, 2021. The influence of spaceflight and simulated microgravity on bacterial motility and chemotaxis. NPJ Microgravity, 7(1):7.
https://doi.org/10.1038/s41526-021-00135-x

Adamopoulos K, Koutsouris D, Zaravinos A, et al., 2021. Gravitational influence on human living systems and the evolution of species on earth. Molecules, 26(9)
https://doi.org/10.3390/molecules26092784

Alvarado-Estrada K, Marenco-Hillembrand L, Maharjan S, et al., 2021. Circulatory shear stress induces molecular changes and side population enrichment in primary tumor-derived lung cancer cells with higher metastatic potential. Sci Rep, 11(1):2800.
https://doi.org/10.1038/s41598-021-82634-1

Amelink A, Kaspers OP, Sterenborg HJ, et al., 2008. Non-invasive measurement of the morphology and physiology of oral mucosa by use of optical spectroscopy. Oral Oncol, 44(1):65-71.
https://doi.org/10.1016/j.oraloncology.2006.12.011

Arun RP, Sivanesan D, Vidyasekar P, et al., 2017. Pten/foxo3/akt pathway regulates cell death and mediates morphogenetic differentiation of colorectal cancer cells under simulated microgravity. Sci Rep, 7(1):5952.
https://doi.org/10.1038/s41598-017-06416-4

Atcha H, Jairaman A, Holt JR, et al., 2021. Mechanically activated ion channel piezo1 modulates macrophage polarization and stiffness sensing. Nat Commun, 12(1):3256.
https://doi.org/10.1038/s41467-021-23482-5

Banyard J, Bielenberg DR, 2015. The role of emt and met in cancer dissemination. Connect Tissue Res, 56(5):403-413.
https://doi.org/10.3109/03008207.2015.1060970

Binnewies M, Roberts EW, Kersten K, et al., 2018. Understanding the tumor immune microenvironment (time) for effective therapy. Nat Med, 24(5):541-550.
https://doi.org/10.1038/s41591-018-0014-x

Bonfiglio T, Biggi F, Bassi AM, et al., 2019. Simulated microgravity induces nuclear translocation of bax and bcl-2 in glial cultured c6 cells. Heliyon, 5(6):e01798.
https://doi.org/10.1016/j.heliyon.2019.e01798

Bootman MD, Bultynck G, 2020. Fundamentals of cellular calcium signaling: A primer. Cold Spring Harb Perspect Biol, 12(1)
https://doi.org/10.1101/cshperspect.a038802

Breslin S, O'driscoll L, 2013. Three-dimensional cell culture: The missing link in drug discovery. Drug Discov Today, 18(5-6):240-249.
https://doi.org/10.1016/j.drudis.2012.10.003

Caulier A, Jankovsky N, Demont Y, et al., 2020. Piezo1 activation delays erythroid differentiation of normal and hereditary xerocytosis-derived human progenitor cells. Haematologica, 105(3):610-622. https://doi.org/10.3324/haematol.2019.218503

Chen X, Wanggou S, Bodalia A, et al., 2018. A feedforward mechanism mediated by mechanosensitive ion channel piezo1 and tissue mechanics promotes glioma aggression. Neuron, 100(4):799-815 e797. https://doi.org/10.1016/j.neuron.2018.09.046

Coste B, Mathur J, Schmidt M, et al., 2010. Piezo1 and piezo2 are essential components of distinct mechanically activated cation channels. Science, 330(6000):55-60. https://doi.org/10.1126/science.1193270

Coste B, Xiao B, Santos JS, et al., 2012. Piezo proteins are pore-forming subunits of mechanically activated channels. Nature, 483(7388):176-181. https://doi.org/10.1038/nature10812

Culliton K, Louati H, Laneuville O, et al., 2021. Six degrees head-down tilt bed rest caused low-grade hemolysis: A prospective randomized clinical trial. NPJ Microgravity, 7(1):4. https://doi.org/10.1038/s41526-021-00132-0

De Palma M, Hanahan D, 2024. Milestones in tumor vascularization and its therapeutic targeting. Nat Cancer, 5(6):827-843. https://doi.org/10.1038/s43018-024-00780-7

De Stefani D, Bononi A, Romagnoli A, et al., 2012. Vdac1 selectively transfers apoptotic ca2+ signals to mitochondria. Cell Death Differ, 19(2):267-273. https://doi.org/10.1038/cdd.2011.92

Den Uil SH, Van Den Broek E, Coupe VMH, et al., 2019. Prognostic value of microvessel density in stage ii and iii colon cancer patients: A retrospective cohort study. BMC Gastroenterol, 19(1):146. https://doi.org/10.1186/s12876-019-1063-4

Deng B, Liu R, Tian X, et al., 2019. Simulated microgravity inhibits the viability and migration of glioma via fak/rhoa/rock and fak/nek2 signaling. In Vitro Cell Dev Biol Anim, 55(4):260-271. https://doi.org/10.1007/s11626-019-00334-7

Dietz C, Infanger M, Romswinkel A, et al., 2019. Apoptosis induction and alteration of cell adherence in human lung cancer cells under simulated microgravity. Int J Mol Sci, 20(14) https://doi.org/10.3390/ijms20143601

Dombroski JA, Hope JM, Sarna NS, et al., 2021. Channeling the force: Piezo1 mechanotransduction in cancer metastasis. Cells, 10(11) https://doi.org/10.3390/cells10112815

Fang C, Liu S, Zhang S, et al., 2025. Jianpi huayu decoction enhances the antitumor effect of doxorubicin via piezo1-mediated autophagy in hepatocellular carcinoma. Phytomedicine, 143:156908. https://doi.org/10.1016/j.phymed.2025.156908

Friedrich EE, Hong Z, Xiong S, et al., 2019. Endothelial cell piezo1 mediates pressure-induced lung vascular hyperpermeability via disruption of adherens junctions. Proc Natl Acad Sci U S A, 116(26):12980-12985.
https://doi.org/10.1073/pnas.1902165116

Globus RK, Morey-Holton E, 2016. Hindlimb unloading: Rodent analog for microgravity. J Appl Physiol (1985), 120(10):1196-1206.
https://doi.org/10.1152/japplphysiol.00997.2015

Grimm D, Wehland M, Corydon TJ, et al., 2020. The effects of microgravity on differentiation and cell growth in stem cells and cancer stem cells. Stem Cells Transl Med, 9(8):882-894.
https://doi.org/10.1002/sctm.20-0084

Grimm D, 2021. Microgravity and space medicine. Int J Mol Sci, 22(13)
https://doi.org/10.3390/ijms22136697

Grimm D, 2022. Microgravity and space medicine 2.0. Int J Mol Sci, 23(8)
https://doi.org/10.3390/ijms23084456

Gudipaty SA, Lindblom J, Loftus PD, et al., 2017. Mechanical stretch triggers rapid epithelial cell division through piezo1. Nature, 543(7643):118-121.
https://doi.org/10.1038/nature21407

Han Y, Liu C, Zhang D, et al., 2019. Mechanosensitive ion channel piezo1 promotes prostate cancer development through the activation of the akt/mtor pathway and acceleration of cell cycle. Int J Oncol, 55(3):629-644.
https://doi.org/10.3892/ijo.2019.4839

Hasegawa K, Fujii S, Matsumoto S, et al., 2021. Yap signaling induces piezo1 to promote oral squamous cell carcinoma cell proliferation. J Pathol, 253(1):80-93.
https://doi.org/10.1002/path.5553

Hope JM, Lopez-Cavestany M, Wang W, et al., 2019. Activation of piezo1 sensitizes cells to trail-mediated apoptosis through mitochondrial outer membrane permeability. Cell Death Dis, 10(11):837.
https://doi.org/10.1038/s41419-019-2063-6

Huang Z, Sun Z, Zhang X, et al., 2019. Loss of stretch-activated channels, piezos, accelerates non-small cell lung cancer progression and cell migration. Biosci Rep, 39(3)
https://doi.org/10.1042/BSR20181679

Hughes-Fulford M, Chang TT, Martinez EM, et al., 2015. Spaceflight alters expression of microrna during t-cell activation. FASEB J, 29(12):4893-4900.
https://doi.org/10.1096/fj.15-277392

Hybel TE, Dietrichs D, Sahana J, et al., 2020. Simulated microgravity influences vegf, mapk, and pam signaling in prostate cancer cells. Int J Mol Sci, 21(4)
https://doi.org/10.3390/ijms21041263

Jeong AJ, Kim YJ, Lim MH, et al., 2018. Microgravity induces autophagy via mitochondrial dysfunction in human hodgkin's lymphoma cells. Sci Rep, 8(1):14646.
https://doi.org/10.1038/s41598-018-32965-3

Jiang F, Yin K, Wu K, et al., 2021. The mechanosensitive piezo1 channel mediates heart mechano-chemo transduction. Nat Commun, 12(1):869.
https://doi.org/10.1038/s41467-021-21178-4

Jiang Z, Chen J, 2022. [anti-angiogenesis in lung cancer: Current situation, progress and confusion]. Zhongguo Fei Ai Za Zhi, 25(4):278-286.
https://doi.org/10.3779/j.issn.1009-3419.2022.101.16

Kalluri R, Weinberg RA, 2009. The basics of epithelial-mesenchymal transition. J Clin Invest, 119(6):1420-1428.
https://doi.org/10.1172/JCI39104

Kimlin LC, Casagrande G, Virador VM, 2013. In vitro three-dimensional (3d) models in cancer research: An update. Mol Carcinog, 52(3):167-182.
https://doi.org/10.1002/mc.21844

Kuntze A, Goetsch O, Fels B, et al., 2020. Protonation of piezo1 impairs cell-matrix interactions of pancreatic stellate cells. Front Physiol, 11:89.
https://doi.org/10.3389/fphys.2020.00089

Lee JE, Kim MY, 2022. Cancer epigenetics: Past, present and future. Semin Cancer Biol, 83:4-14.
https://doi.org/10.1016/j.semcancer.2021.03.025

Lewis ML, Reynolds JL, Cubano LA, et al., 1998. Spaceflight alters microtubules and increases apoptosis in human lymphocytes (jurkat). FASEB J, 12(11):1007-1018.
https://doi.org/10.1096/fasebj.12.11.1007

Li C, Rezania S, Kammerer S, et al., 2015. Piezo1 forms mechanosensitive ion channels in the human mcf-7 breast cancer cell line. Sci Rep, 5:8364.
https://doi.org/10.1038/srep08364

Li J, Li X, Tong X, et al., 2018. Investigation of the optimal duration of bed rest in the supine position to reduce complications after lumbar puncture combined with intrathecal chemotherapy: A multicenter prospective randomized controlled trial. Support Care Cancer, 26(9):2995-3002.
https://doi.org/10.1007/s00520-018-4142-0

Lin YC, Guo YR, Miyagi A, et al., 2019. Force-induced conformational changes in piezo1. Nature, 573(7773):230-234.
https://doi.org/10.1038/s41586-019-1499-2

Liu ZL, Chen HH, Zheng LL, et al., 2023. Angiogenic signaling pathways and anti-angiogenic therapy for cancer. Signal Transduct Target Ther, 8(1):198.
https://doi.org/10.1038/s41392-023-01460-1

Lopes-Coelho F, Martins F, Pereira SA, et al., 2021. Anti-angiogenic therapy: Current challenges and future perspectives. Int J Mol Sci, 22(7)
https://doi.org/10.3390/ijms22073765

Massey A, Stewart J, Smith C, et al., 2024. Mechanical properties of human tumour tissues and their implications for cancer development. Nat Rev Phys, 6(4):269-282.
https://doi.org/10.1038/s42254-024-00707-2

Nourse JL, Pathak MM, 2017. How cells channel their stress: Interplay between piezo1 and the cytoskeleton. Semin Cell Dev Biol, 71:3-12.
https://doi.org/10.1016/j.semcdb.2017.06.018

Ploutz-Snyder L, 2016. Evaluating countermeasures in spaceflight analogs. J Appl Physiol (1985), 120(8):915-921.
https://doi.org/10.1152/japplphysiol.00860.2015

Prasad B, Grimm D, Strauch SM, et al., 2020a. Influence of microgravity on apoptosis in cells, tissues, and other systems in vivo and in vitro. Int J Mol Sci, 21(24)
https://doi.org/10.3390/ijms21249373

Prasad B, Richter P, Vadakedath N, et al., 2020b. Exploration of space to achieve scientific breakthroughs. Biotechnol Adv, 43:107572.
https://doi.org/10.1016/j.biotechadv.2020.107572

Ren ZH, Hu CY, He HR, et al., 2020. Global and regional burdens of oral cancer from 1990 to 2017: Results from the global burden of disease study. Cancer Commun (Lond), 40(2-3):81-92.
https://doi.org/10.1002/cac2.12009

Romani P, Valcarcel-Jimenez L, Frezza C, et al., 2021. Crosstalk between mechanotransduction and metabolism. Nat Rev Mol Cell Biol, 22(1):22-38.
https://doi.org/10.1038/s41580-020-00306-w

Sasahira T, Kirita T, 2018. Hallmarks of cancer-related newly prognostic factors of oral squamous cell carcinoma. Int J Mol Sci, 19(8)
https://doi.org/10.3390/ijms19082413

Singh R, Rajput M, Singh RP, 2021. Simulated microgravity triggers DNA damage and mitochondria-mediated apoptosis through ros generation in human promyelocytic leukemic cells. Mitochondrion, 61:114-124.
https://doi.org/10.1016/j.mito.2021.09.006

Song Y, Chen J, Zhang C, et al., 2022. Mechanosensitive channel piezo1 induces cell apoptosis in pancreatic cancer by ultrasound with microbubbles. iScience, 25(2):103733.
https://doi.org/10.1016/j.isci.2022.103733

Sun Y, Li M, Liu G, et al., 2020. The function of piezo1 in colon cancer metastasis and its potential regulatory mechanism. J Cancer Res Clin Oncol, 146(5):1139-1152.
https://doi.org/10.1007/s00432-020-03179-w

Suzuki T, Muraki Y, Hatano N, et al., 2018. Piezo1 channel is a potential regulator of synovial sarcoma cell-viability. Int J Mol Sci, 19(5)
https://doi.org/10.3390/ijms19051452

Takahashi K, Takahashi H, Furuichi T, et al., 2021. Gravity sensing in plant and animal cells. NPJ Microgravity, 7(1):2.
https://doi.org/10.1038/s41526-020-00130-8

Tan Y, Wang Z, Xu M, et al., 2023. Oral squamous cell carcinomas: State of the field and emerging directions. Int J Oral Sci, 15(1):44.
https://doi.org/10.1038/s41368-023-00249-w

Tijore A, Yao M, Wang YH, et al., 2021. Selective killing of transformed cells by mechanical stretch. Biomaterials, 275:120866.
https://doi.org/10.1016/j.biomaterials.2021.120866

Vidyasekar P, Shyamsunder P, Arun R, et al., 2015. Genome wide expression profiling of cancer cell lines cultured in microgravity reveals significant dysregulation of cell cycle and microrna gene networks. PLoS One, 10(8):e0135958.
https://doi.org/10.1371/journal.pone.0135958

Visvader JE, Lindeman GJ, 2012. Cancer stem cells: Current status and evolving complexities. Cell Stem Cell, 10(6):717-728.
https://doi.org/10.1016/j.stem.2012.05.007

Xu X, Liu S, Liu H, et al., 2021. Piezo channels: Awesome mechanosensitive structures in cellular mechanotransduction and their role in bone. Int J Mol Sci, 22(12)
https://doi.org/10.3390/ijms22126429

Yu L, Su Z, Tian D, et al., 2025. Piezo1 induces mitochondrial autophagy dysfunction leading to cartilage injury in knee osteoarthritis. Mol Med, 31(1):272.
https://doi.org/10.1186/s10020-025-01335-x

Zong B, Yu F, Zhang X, et al., 2023. Mechanosensitive piezo1 channel in physiology and pathophysiology of the central nervous system. Ageing Res Rev, 90:102026.
https://doi.org/10.1016/j.arr.2023.102026

Supplementary information
Material and methods; Figs. S1–S7; Tables S1 and S2

Supplementary information:

Material and methods

Cell Culture, Transfection

The human OSCC cell lines Cal-27, HSC-3 (high metastatic potential), and HSC-4(low metastatic potential) were obtained from the American Type Culture Collection (ATCC) and maintained in Dulbecco's Modified Eagle's Medium (DMEM) supplemented with 10% fetal bovine serum (FBS) and 1% penicillin-streptomycin, in a humidified atmosphere at 37°C with 5% CO2. Cells were cultured in T-75 flasks and passaged using trypsin-EDTA solution when they reached 80% confluence. The culture medium was changed every 2 – 3 days, and cell morphology was regularly monitored under an inverted phase-contrast microscope. The mouse OSCC cell line 4MOSC1 was derived as previously described and cultured in Defined Keratinocyte SFM (ThermoFisher, 10744019) supplemented with 5 ng/mL EGF Recombinant Mouse Protein (ThermoFisher, #PMG8041), 0.0001 nM/mL Cholera Toxin (Sigma-Aldrich, C8052), and 1% penicillin/streptomycin (Sigma-Aldrich, A5955).

The siRNA sequences used in this study were designed to target Piezo1 and synthesized by Transsheep according to the following sequences: F-CCAAGTACTGGATCTATGT and R-GCAAGTTCGTGCGCGGATT. siRNA transfection was performed using Lipofectamine 3000 (ThermoFisher) for 12 or 24 hours, following the manufacturer's instructions.

The Rotary Cell Culture System (RCCS, Synthecon, RCCS-4D)

Cells were divided into SMG and NG groups. Cells in the NG group were cultured using the standard method described above. For the SMG group, cells were passaged at an appropriate concentration into disposable vessels and cultured in the RCCS following the manufacturer's instructions. During the first five minutes of culture, the RCCS speed was set to 8 RPM; after 5 minutes, the rotation speed was increased to 14 RPM. Cells were continuously cultured in disposable vessels for 48 hours before sampling for subsequent analysis.

Cell scratch assay

Cells were seeded in 6-well plates and allowed to reach confluence. A standardized wound was created in the cell monolayer using a sterile 200 μL pipette tip. The cells were then washed with phosphate-buffered saline (PBS) to remove debris and floating cells. For the scratch and cell viability assays and colony formation assay following microgravity simulation, cells (3D spheroids from SMG and monolayers from NG) were harvested and dissociated into single-cell suspensions using 0.25% Trypsin-EDTA. The cells were immediately reseeded into 6- or 96-well plates under NG conditions. The assays commenced once the cells had successfully adhered to the plate surface, allowing us to evaluate the sustained effects of the prior microgravity exposure. The cells were then treated under the appropriate experimental conditions. Images of the scratch were captured at 24 hours to assess cell migration into the wound area. The scratch width was measured at each time point using image analysis software (ImageJ).

Colony formation assay

Cells were trypsinized and resuspended in complete growth medium to obtain a single-cell suspension. The suspension was then seeded into 6-well plates (500 cells per well) to allow colony formation. The plates were gently rocked to ensure even cell distribution. The cells were incubated in a humidified atmosphere at 37°C with 5% CO2 for 7 – 14 days to facilitate colony formation, with medium changes every 2 – 3 days during the

incubation period. Following incubation, the cells were fixed with 4% paraformaldehyde (PFA) and stained with crystal violet to visualize the colonies. The number of colonies in each well was counted manually or using ImageJ.

Cell viability assay

Cells were first cultured (in RCCS vessels) under NG or SMG conditions for the indicated durations. Subsequently, cells were harvested, dissociated, and seeded in 96-well plates at 5000 cells per well in complete growth medium and incubated at 37 °C with 5% CO2. Following incubation, the cells were subjected to rotational stimulation using a rotational device at a specified duration and speed. Control wells were left unstimulated. Following stimulation, Cell Counting Kit-8 (CCK-8) reagent (Beyotime, China) was added to each well according to the manufacturer's instructions.

Western blotting

The knockdown of the target gene by Piezo1 siRNA transfection and the expression of autophagy markers were analyzed using Western blotting. Transfected cells were lysed in RIPA buffer (Sigma-Aldrich) containing Halt™ protease inhibitor (ThermoFisher). The lysates were centrifuged at 12,000× g for 10 minutes at 4°C. The total protein concentration was determined using a BSA protein standard kit (ThermoFisher). Protein samples were electrophoresed on a 10% PAGE gel (120 V for 1.5 hours) and transferred to nitrocellulose membranes (Pall Corp) for 1.5 hours at 300 mA. Protein blots were detected using SuperSignal® West Pico (ThermoFisher) and the following antibodies: Piezo1 (Proteintech, 82625-4-RR, 1:1000), LC3A (Proteintech, 18722-1-AP, 1:1000), LC3B (Proteintech, 18725-1-AP, 1:1000), P62 (Proteintech, 31403-1-AP, 1:1000), ATG9B (ThermoFisher, PA5-20998, 2 μg/ml), PARKIN(Proteintech, 14060-1-AP, 1:2000), PINK1(Proteintech, 23274-1-AP, 1:2000), GAPDH (Proteintech, 10494-1-AP, 1:5000), and secondary antibodies goat anti-mouse IgG (ThermoFisher, 31430) or goat anti-mouse IgG (ThermoFisher, 31460).

Membrane potential damage assessment

Cells were incubated for 20 mins at 37°C with Rhodamine 123 Kits (Beyotime, C2008S) loaded with dyes using Carbonyl Cyanide m-Chlorophenylhydrazone (CCCP) as a positive control. The results were detected using a confocal microscope and fluorescence quantification by Zen Lite 3.4.

Measurement of mitochondrial calcium

Cells were incubated for 30 minutes at 37°C in DMEM with 10% FBS, supplemented with MitoTracker GFP (ThermoFisher, 50 nM) and Rhod-2 AM (ThermoFisher, 0.4 mM, incubated overnight), according to the manufacturer's instructions. This experimental setup enables real-time visualization and dynamic monitoring of immunofluorescence-labeled structures or proteins in live cells using the Zeiss LSM980 confocal microscope, which offers live-cell imaging capabilities.

Mitochondrial autophagy fluorescence

After packaging the pTSBX-StubRFP-SensGFP-LC3B-IRES-puro-EFS-Mito-BFP-TSB vector into lentivirus (Transheep, China) and infecting cells at an MOI of 10, the cells were subjected to puromycin selection at 2 μg/ml for three generations. The expression of the three fluorescent proteins (blue for mitochondria, red and green for LC3B dual-color) was then confirmed using a fluorescence microscope. Fluorescence imaging was performed using a confocal microscope, and fluorescence intensity was quantified using Zen Lite 3.4. The following antibodies were used for IF: PARKIN (Proteintech, 14060-1-AP, 1:200),

PINK1 (Proteintech, 23274-1-AP, 1:200), TOM20 (Proteintech, 66777-1-1g, 1:500).

RNA-seq

Total RNA from HSC-3 cells was extracted using the TRIzol reagent (Invitrogen, CA, USA) according to the manufacturer ' s protocol. RNA purity and quantification were evaluated using the NanoDrop 2000 spectrophotometer (Thermo Scientific, USA). RNA integrity was assessed using the Agilent 2100 Bioanalyzer (Agilent Technologies, Santa Clara, CA, USA).

The libraries were then constructed using the VAHTS Universal V6 RNA-seq Library Prep Kit according to the manufacturer's instructions. The transcriptome sequencing and analysis were conducted by OE Biotech Co., Ltd. (Shanghai, China). The libraries were sequenced on the Illumina Novaseq 6000 platform, and 150 bp paired-end reads were generated.

The sequencing-generated FASTQ files were evaluated for read quality and mapping rate using FastQC (version 0.11.9). Clean reads were aligned to the hg38 reference genome using Hisat2 (version 2.1.0). FPKM of each gene was calculated, and the read count of each gene was obtained by HTSeq-count (Version0.11.2). PCA analysis was performed using R (Version 3.2.0) to evaluate the biological duplication of samples. Differential expression analysis was performed using DESeq2. Q value < 0.05 and foldchange > 2 or foldchange < 0.5 were set as the thresholds for significantly differentially expressed genes (DEGs). Hierarchical cluster analysis of DEGs was performed in R (Version 3.2.0) to visualize gene expression patterns across groups and samples.

Based on the hypergeometric distribution, GO, KEGG pathway, Reactome, and WikiPathways enrichment analyses of DEGs were performed in R (Version 3.2.0) to identify significantly enriched terms. R was used to draw the column diagram, the chord diagram, and the bubble diagram of the significant enrichment term.

4MOSC1 tumor formation in vivo

All animal studies related to oral carcinogenesis were approved by the Institutional Animal Care and Use Committee (IACUC) of Zhejiang University, Hangzhou. Mice were housed in micro-isolators and individually ventilated cages at the Animal Center, with access to acidified water and a standard lab diet. The temperature in the animal facility was maintained between 65°F and 75°F (~18–23°C) with 40%–60% humidity. All animal handling procedures were performed in laminar flow hoods. Personnel were required to wear scrubs, lab coats, masks, hairnets, dedicated shoes, and disposable gloves when entering the animal rooms. 4MOSC1 cells (0.5 million per mouse) were transplanted into the tongues of female C57Bl/6 mice (4–6 weeks old, weighing 16–18 g). The mice were randomly assigned to experimental groups once tumors had formed (on days 5–6).

Simulating microgravity in hindlimb unloading mice

To simulate microgravity, the HU model was established following standard protocols. Mice were individually housed in specialized suspension cages. Briefly, a traction loop was applied to the tail and connected to the suspension system. The suspension height was carefully adjusted to elevate the hindlimbs, maintaining a head-down tilt of approximately 30 degrees. This specific angle ensured that the forelimbs remained in firm contact with the cage grid, allowing the mice to access food and water and groom normally, while the hindlimbs remained non-weight bearing. The mice were monitored daily to ensure the suspension angle was maintained.

Drug treatment for mice

For drug treatment, the mice were given either an intraperitoneal (IP) injection of saline as a control or Dooku1 (MedChemExpress # HY-126010, 10 μM per mouse, three times a week) for 10 days. The mice were then euthanized following treatment completion (or when control-treated mice succumbed to tumor burdens, as

determined by the ASP guidelines), and tumors were dissected for histologic and immunohistochemical evaluation.

Histological analyses

The tongue samples were fixed in 4% Paraformaldehyde Fix Solution (Servicebio, China) for 24 hours at room temperature, dehydrated in graded ethanol, and embedded in paraffin. The tissue was then sectioned into 5 μm slices using a microtome (Leica) and stained with HE.

For immunohistochemistry, the tumor section slides confirmed by HE staining were deparaffinized in xylene for 30 minutes and rehydrated using graded ethanol. Epitope retrieval was performed using a pressure cooker for 2.5 minutes. After blocking endogenous peroxidase activity with hydrogen peroxide (Beyotime), sections were incubated overnight at 4°C with Ki-67 antibody (Proteintech, 27309-1-AP, 1:200) and CD34 antibody (Proteintech, 31120-1-AP, 1:150). After washing, the sections were incubated with goat anti-mouse IgG antibody (ThermoFisher, 31430, 1:1500) for 30 minutes at room temperature. Following immunostaining, the slides were counterstained with hematoxylin for 20 seconds to visualize the nuclei and differentiated in acid alcohol or tap water to remove any excess. DAB (Beyotime, P0203) was used for color development according to the manufacturer's instructions.

Data collection and processing of TCGA

Survival Genie includes 53 datasets across 27 distinct malignancies from 11 different cancer programs, covering both adult and pediatric cancers. All clinical and genomic data were downloaded from the GDC data portal using the Genomic Data Commons Bioconductor R package. TCGAplot (Version 8.0.0) was used for Pan-cancer expression analysis.

Survival Genie performs statistical analysis of overall survival (OS) and disease-free survival (DFS) using the R package 'survival'. Kaplan–Meier survival curves are generated to estimate OS/DFS using the survfit function, and a log-rank test is performed to compare OS/DFS between defined high- and low-risk groups. Univariate analysis using the Cox proportional hazards regression model is conducted on patient data with the Coxph function in R/Bioconductor. A survival association is considered significant if the P-values for both the log-rank and Wald tests are less than 0.05.

Statistical analysis

For in vitro assays, experiments were performed in biological triplicates and technical duplicates. All experiments were pooled for statistical analysis. For in vivo experiments, each independent experiment included 10 mice per group. Data are presented as means, with error bars representing standard deviation (SD). Statistical differences between groups were analyzed using Student's t-test or one-way analysis of variance (ANOVA), followed by Tukey's or Dunnett's multiple comparison tests. $P < 0.05$ was considered statistically significant. All statistical analyses were conducted using GraphPad Prism software.

Figs. S1–S7
Table S1–S2

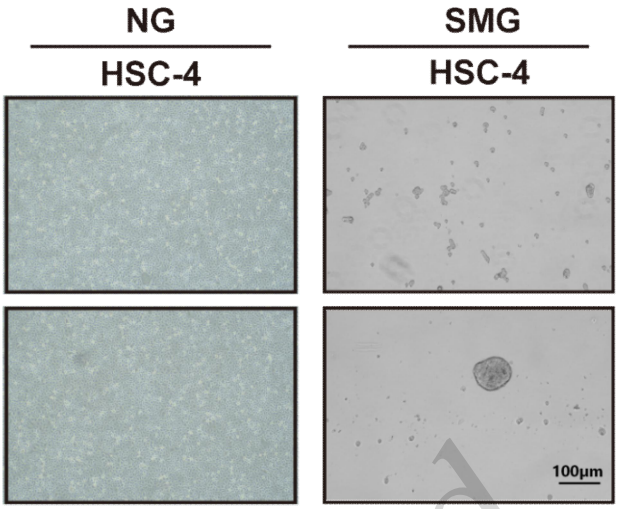

Fig. S1 Effects of simulated microgravity on OSCC cell morphology. HSC-4 cells cultured under normal gravity (NG) conditions exhibit typical adherent growth, while cells exposed to simulated microgravity (SMG) for 48 hours adopt irregular shapes and reassemble into three-dimensional multicellular spheroid structures.

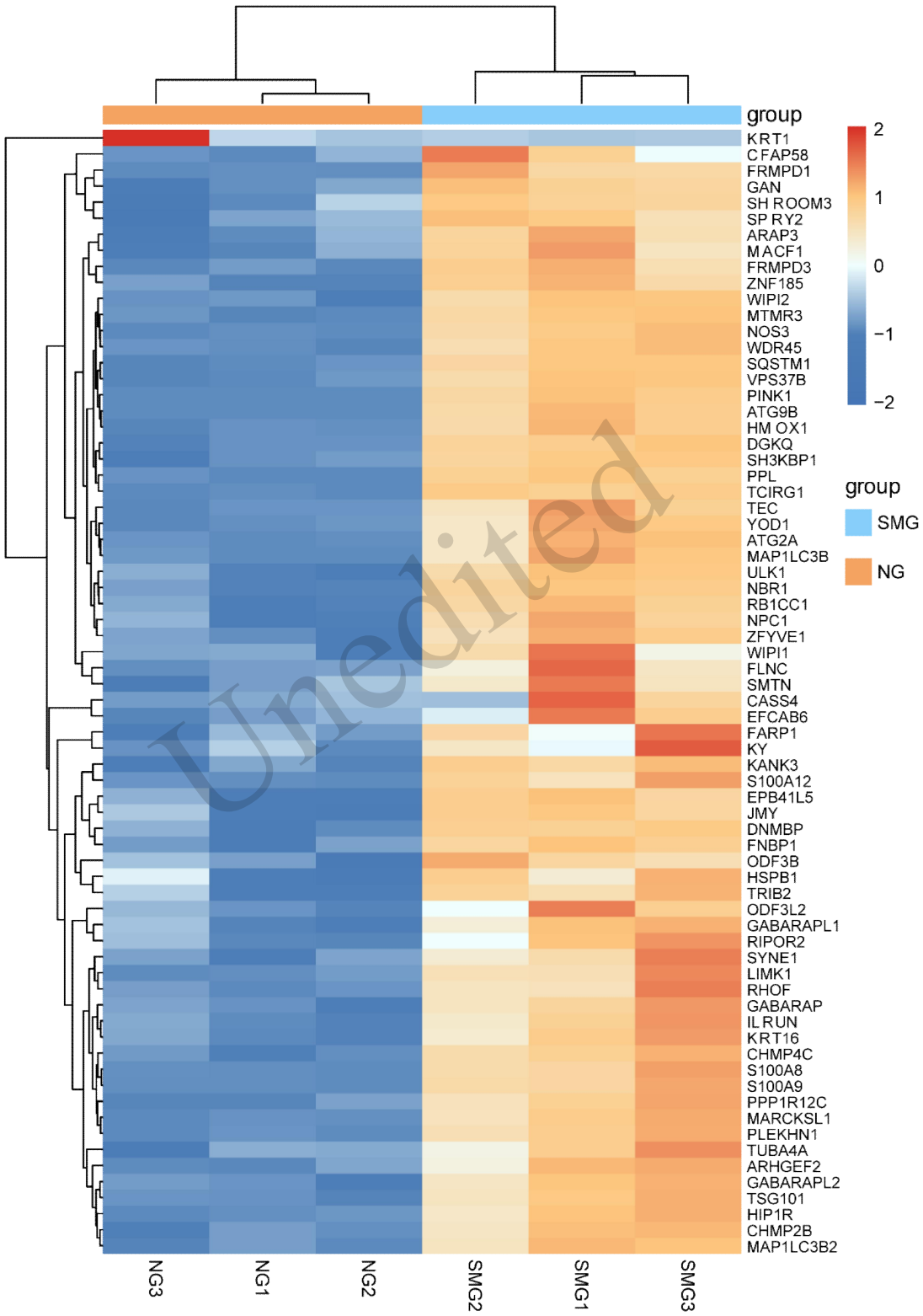

Fig. S2 Hierarchical clustering heatmap of differentially expressed genes in HSC-3 cells under normal gravity (NG) and simulated microgravity (SMG) conditions. The heatmap illustrates the differential expression profiles of HSC-3 cells following 48 hours of culture. Columns represent independent biological replicates (n=3) for the NG (left) and SMG (right) groups, while rows represent individual

genes. The color scale indicates the relative expression levels (Z-score normalized): red indicates upregulation (high expression) and blue indicates downregulation (low expression). Both samples and genes are organized based on hierarchical clustering (dendrograms on the top and left). Notably, a cluster of genes associated with autophagy and mitophagy (e.g., *ATG9B*, *PINK1*, *MAP1LC3B*, *SQSTM1*) exhibits significant upregulation in the SMG group compared to the NG group.

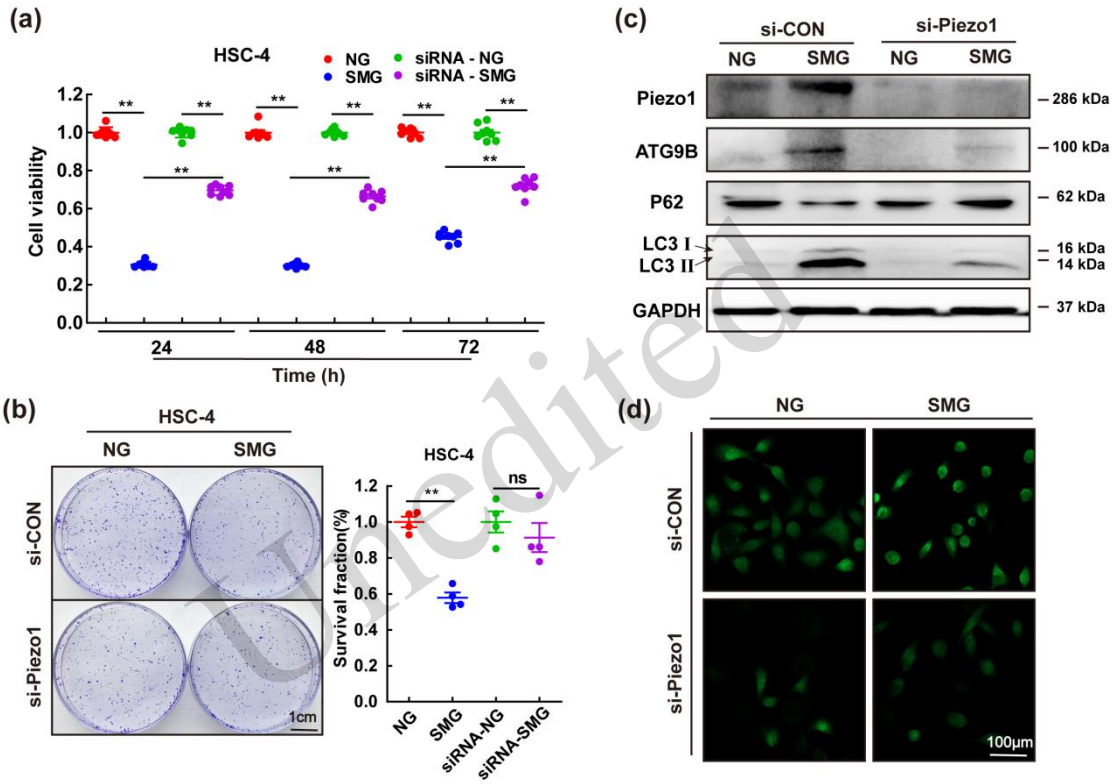

Fig. S3 SMG-induced mitophagy in HSC-4 cells via Piezo1 regulation. (a-c) the recovery of cell viability (n=8) (a) colony formation ability (n=4) (b) of si-Piezo1 siRNA in the SMG stimulated HSC-4. (c) Autophagy-related key genes ATG9B, LC3, and Piezo1 were recovered by the siRNA knockdown after SMG. (d): the confocal images show the calcium ion fluorescence in each group. Data are expressed as mean±standard deviation (SD). ns, not significant, * *P*<0.05, ** *P*<0.01.

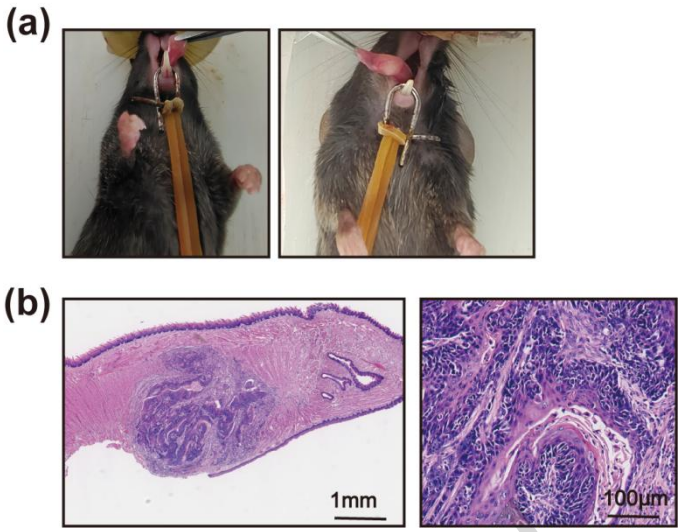

Fig. S4 Tumor-bearing model in a tongue in C57b mice. (a) On day 7, after the injection of 4MOSC1, an obvious tumor formed in the tongue. (b) The tumors are confirmed as OSCC in HE slides. 4MOSC1: 4-Nitroquinoline 1-Oxide Induced Mouse Oral Squamous Cell Carcinoma1, OSCC: Oral Squamous Cell Carcinoma.

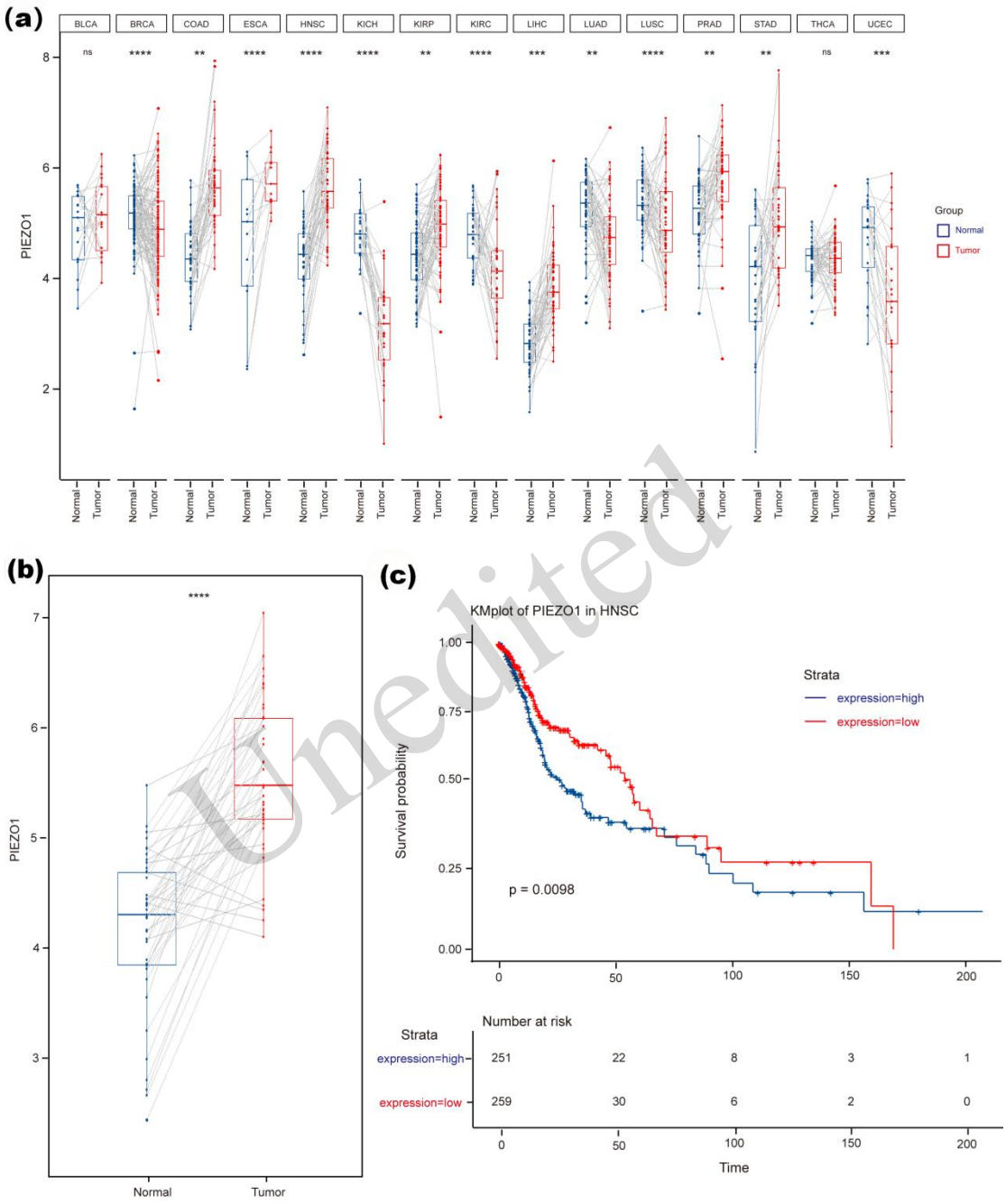

Fig. S5 PIEZO1 expression in Pan-Cancer data from the TCGA project. (a) *PIEZO1* expression level in TCGA tumors, abbreviations of pan-cancer were in Table S1. (b) Box plot data of *PIEZO1* expression in HNSC. (c) Prognostic value of PIEZO1 in HNSC based on Kaplan-Meier analysis. High expression of *PIEZO1* was associated with poor overall survival in patients with HNSC (n=510). HNSC: Head and Neck Symptom Checklist, PIEZO1: Piezo Type Mechanosensitive Ion Channel Component 1.

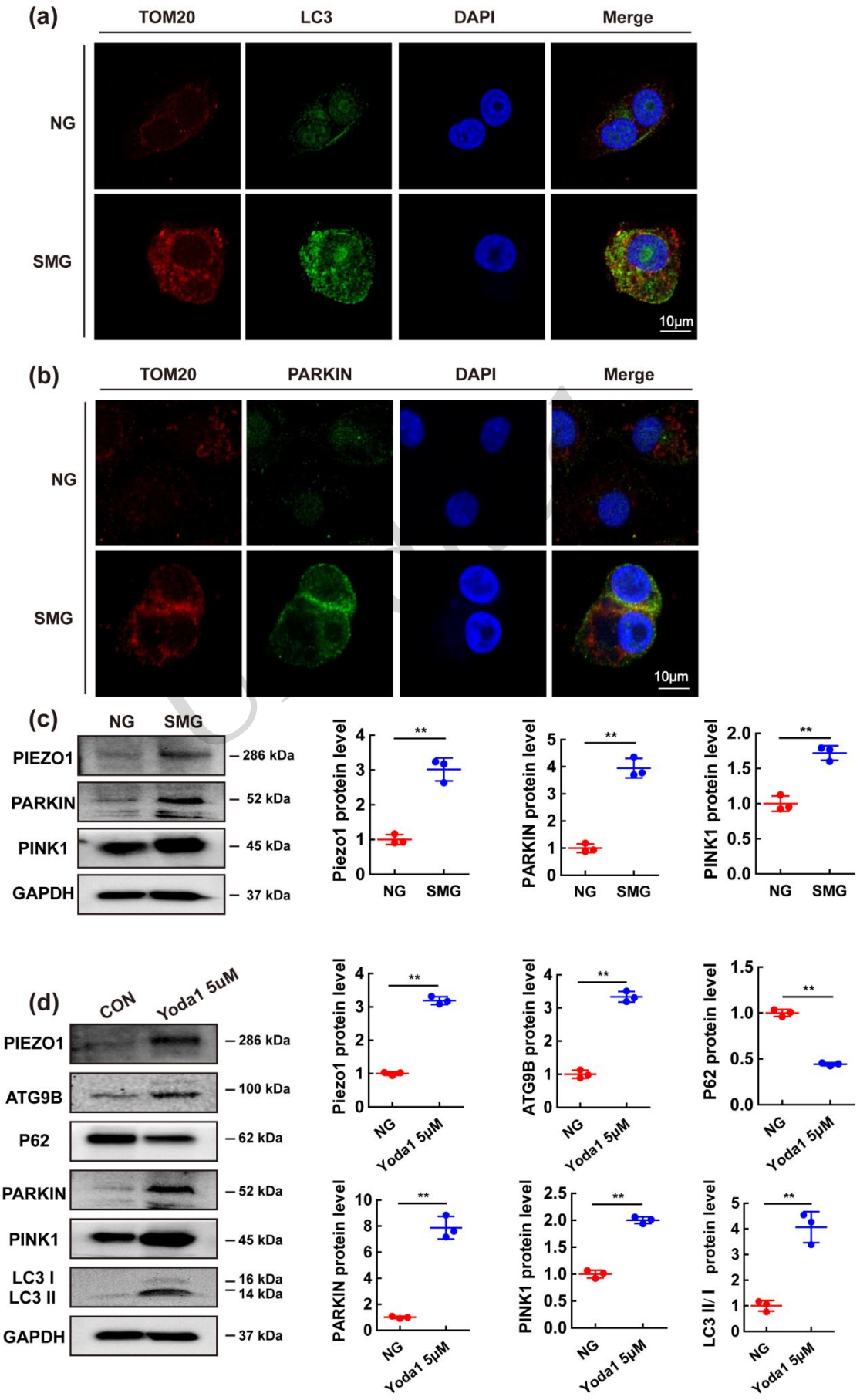
(a)
TOM20
LC3
DAPI
Merge
NG
SMG
10μm
(b)
TOM20
PARKIN
DAPI
Merge
NG
SMG
10μm
(c)
NG
SMG
PIEZO1
PARKIN
PINK1
GAPDH
286 kDa
52 kDa
45 kDa
37 kDa
Piezo1 protein level
PARKIN protein level
PINK1 protein level
(d)
CON
Yoda1 5uM
PIEZO1
ATG9B
P62
PARKIN
PINK1
LC3 I
LC3 II
GAPDH
286 kDa
100 kDa
62 kDa
52 kDa
45 kDa
16 kDa
14 kDa
37 kDa
Piezo1 protein level
ATG9B protein level
P62 protein level
PARKIN protein level
PINK1 protein level
LC3 II/ I protein level
NG
Yoda1 5μM

Fig. S6 SMG and Piezo1 activation induce mitophagy via PINK1-Parkin pathway in HSC-3 cells. (a) Representative immunofluorescence images showing the colocalization of mitochondria (TOM20, red) and autophagosomes (LC3, green) in HSC-3 cells under NG and SMG conditions. Nuclei were stained with DAPI (blue). SMG treatment significantly increased the recruitment of LC3 to mitochondria. Scale bar: 10μm. (b) Representative immunofluorescence images showing the colocalization of mitochondria (TOM20, red) and the mitophagy regulator PARKIN (green). SMG treatment induced the translocation of PARKIN to mitochondria compared to the NG group. Scale bar: 10 μm. (c) Western blot analysis and quantification of PIEZO1, PARKIN, and PINK1 expression levels in HSC-3 cells under NG and SMG conditions. SMG significantly upregulated the expression of these mitophagy-related proteins. n=3. (d) Western blot analysis and quantification of PIEZO1 and mitophagy markers (ATG9B, P62, PARKIN, PINK1, LC3) in HSC-3 cells treated with the Piezo1 agonist Yoda1 (5μM). Yoda1 treatment successfully mimicked the SMG-induced upregulation of PIEZO1, ATG9B, PINK1, PARKIN, and LC3-II/LC3-I ratio, and the down-regulation of P62. n=3. Data are expressed as mean±standard deviation (SD). ns, not significant, * *P*<0.05, ** *P*<0.01. TOM20: Translocase of Outer Mitochondrial Membrane 20, PIEZO1: Piezo Type Mechanosensitive Ion Channel Component 1, PARKIN: Parkin RBR E3 Ubiquitin Protein Ligase, PINK1: PTEN Induced Kinase 1, GAPDH: Glyceraldehyde-3-Phosphate Dehydrogenase, ATG9B: Autophagy Related 9B, P62: Sequestosome 1 (also known as SQSTM1), LC3 I: Microtubule-Associated Protein 1 Light Chain 3 Beta I, LC3 II: Microtubule-Associated Protein 1 Light Chain 3 Beta II.

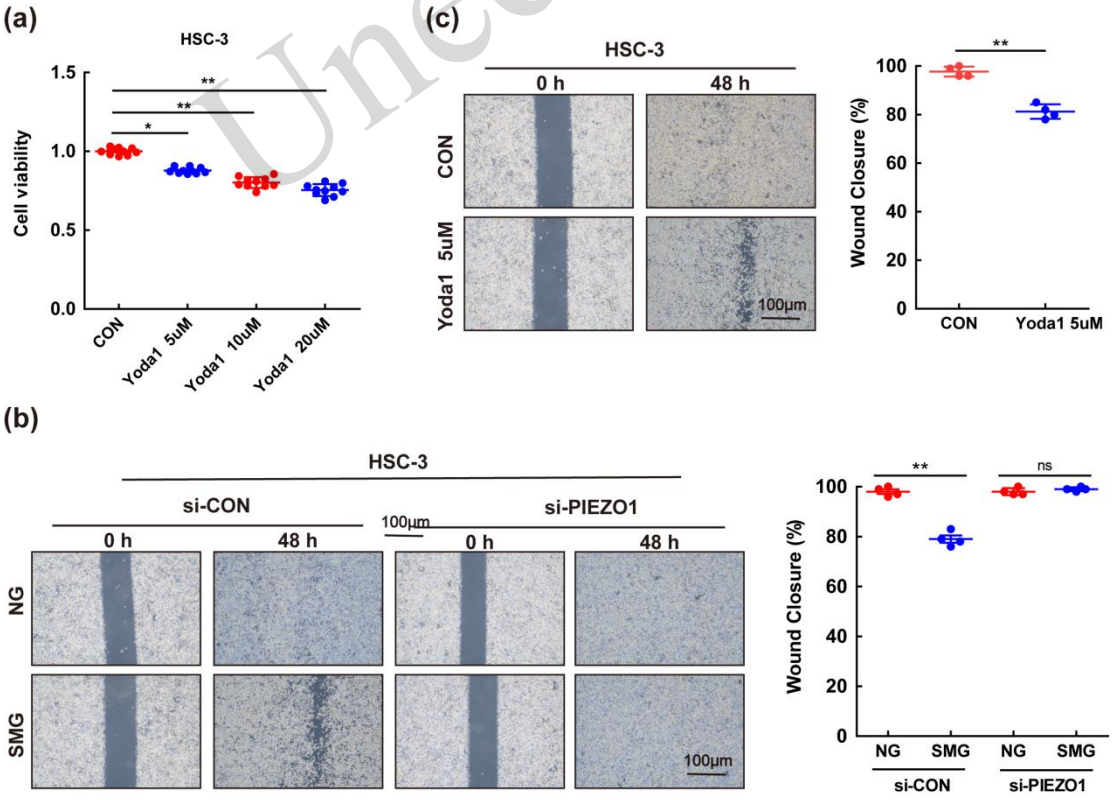

Fig. S7 Piezo1 activation mimics SMG-induced proliferation and migration suppression, knockdown reverses effects. (a) CCK-8 cell viability assay of HSC-3 cells treated with increasing concentrations of the Piezo1 agonist Yoda1 (5, 10, and 20 μM). Yoda1 treatment significantly inhibited cell proliferation in

a dose-dependent manner compared to the control group. n=10. (b) Wound healing migration assay and quantitative analysis of HSC-3 cells transfected with control siRNA (si-CON) or Piezo1 siRNA (si-PIEZO1) under NG and SMG conditions. SMG treatment significantly inhibited wound closure in the si-CON group, whereas Piezo1 knockdown (si-PIEZO1) significantly rescued the migratory capability of cells under SMG conditions. n=4. (c) Wound healing migration assay and quantitative analysis of HSC-3 cells treated with Yoda1 (5μM) compared to the control (CON). Pharmacological activation of Piezo1 by Yoda1 significantly suppressed cell migration, recapitulating the phenotype observed under SMG conditions. n=4. Data are expressed as mean±standard deviation (SD). ns, not significant, * *P*<0.05, ** *P*<0.01.

Table S1 Abbreviations of pan-cancer

Abbreviations	Full names
ACC	Adrenocortical carcinoma
BLCA	Bladder Urothelial Carcinoma
BRCA	Breast invasive carcinoma
CESC	Cervical squamous cell carcinoma and endocervical adenocarcinoma
CHOL	Cholangiocarcinoma
COAD	Colon adenocarcinoma
DLBC	Lymphoid Neoplasm Diffuse Large B-cell Lymphoma
ESCA	Esophageal carcinoma
GBM	Glioblastoma multiforme
HNSC	Head and Neck squamous cell carcinoma
KICH	Kidney Chromophobe
KIRC	Kidney renal clear cell carcinoma
KIRP	Kidney renal papillary cell carcinoma
LAML	Acute Myeloid Leukemia
LGG	Brain Lower Grade Glioma
LIHC	Liver hepatocellular carcinoma
LUAD	Lung adenocarcinoma
LUSC	Lung squamous cell carcinoma
MESO	Mesothelioma
OV	Ovarian serous cystadenocarcinoma
PAAD	Pancreatic adenocarcinoma
PCPG	Pheochromocytoma and Paraganglioma
PRAD	Prostate adenocarcinoma
READ	Rectum adenocarcinoma
SARC	Sarcoma
SKCM	Skin Cutaneous Melanoma

STAD	Stomach adenocarcinoma
TGCT	Testicular Germ Cell Tumors
THCA	Thyroid carcinoma
THYM	Thymoma
UCEC	Uterine Corpus Endometrial Carcinoma
UCS	Uterine Carcinosarcoma
UVM	Uveal Melanoma

Table S2: DEG list of SMG vs. NG (*P*<0.05, log2FoldChange>1 or log2FoldChange<-1)